We are IntechOpen, the world's leading publisher of Open Access books Built by scientists, for scientists

4,800
Open access books available

122,000
International authors and editors

135M
Downloads

Our authors are among the

154
Countries delivered to

TOP 1%
most cited scientists

12.2%
Contributors from top 500 universities

CLARIVATE ANALYTICS BOOK CITATION INDEX INDEXED

WEB OF SCIENCE™

Selection of our books indexed in the Book Citation Index in Web of Science™ Core Collection (BKCI)

Interested in publishing with us?
Contact book.department@intechopen.com

Numbers displayed above are based on latest data collected.
For more information visit www.intechopen.com

Chapter 2

Molecular Microfluidic Bioanalysis: Recent Progress in Preconcentration, Separation, and Detection

Emmanuel Roy, Antoine Pallandre, Bacem Zribi, Marie-Charlotte Horny, François-Damien Delapierre, Andrea Cattoni, Jean Gamby and Anne-Marie Haghiri-Gosnet

Additional information is available at the end of the chapter

http://dx.doi.org/10.5772/65772

Abstract

This chapter reviews the state-of-art of microfluidic devices for molecular bioanalysis with a focus on the key functionalities that have to be successfully integrated, such as preconcentration, separation, signal amplification, and detection. The first part focuses on both passive and electrophoretic separation/sorting methods, whereas the second part is devoted to miniaturized biosensors that are integrated in the last stage of the fluidic device.

Keywords: microfluidic bioanalysis, separation, concentration, on-a-chip optical detection, electrochemical sensors

1. Introduction

Advances in biochemistry and technology for enhancing sensitivity and selectivity of bioanalysis play a central role in clinical chemistry and medical diagnostics. The latter are performed much earlier to prevent disease or in a repetitive manner to define more specific and personal therapies. However, such analytical protocols are often implemented at the macroscale level where large volumes of samples are needed. The development of microfluidic bioanalysis thus becomes important, since these platforms can offer short analysis time to result in volume smaller than 1 μl, low cost, multiplexed analysis of several analytes, and portability. Therefore, the development of extremely sensitive, highly selective, simple, robust and yet inexpensive miniaturized platforms has become essential for a wide range of applications, including clinical diagnostics, environmental monitoring, and food safety testing. This chapter reviews the state-of-art of microfluidic devices for molecular bioanalysis with a focus

on the key functionalities that have been successfully integrated in the chip, such as preconcentration, separation, and detection.

Impressive innovations have been demonstrated allowing selectively sorting, concentrating, and amplifying analytes of interest [1–3]. Therefore, the first section of this chapter mainly targets passive and electrical-based strategies for biomolecular and cellular purification, and concentration toward genomic, proteomic, and metabolite applications. The second part focuses on sensitive and selective detection techniques. Two routes are described: (i) on-chip detection based on nanostructured biophotonic sensors and (ii) electrochemical detection. These sensors are integrated in small microchannels or microchambers where specific enhanced sensing properties are generated. The correlation between the biosensor interface and its microfluidic environment for optimal detection of analytes is reviewed. Fundamental kinetics and mass-transport versus the microfluidic properties in terms of fluidic characteristics is introduced for highly operative and sensitive microfluidic applications.

2. Microfluidic filtration, concentration, and sorting

Molecular extraction and purification from a biofluid for diagnostic and therapeutic purposes using microfluidics are sensitive issues. Such objectives are challenging regarding the manipulation of the complex biofluid system such as blood or sputum. Moreover, the extraction and purification steps are also important for the quality and the pertinence of the analyte identification and quantification. Each progress and advance will definitively help the clinicians for proper medication. The advantages of such a microfluidic device for genomic pathogenic recognition are also of tremendous importance, because such a platform can shorten the sample analysis time compared to classical methods. Conventional processing methods for preconcentration and separation of analytes entail numerous manual and time-consuming steps. Consequently, it requires most often highly skilled operators, who do not always guarantee the absence of mishandling and contaminants. As a unique example of the needs for rapid molecular extraction from blood, sepsis and blood stream infections that are a major cause of death [4] impose daily patient follow-up to doctors in virology and bacteriology. Antimicrobial therapy should thus be curtailed as early as practicable, ideally just after the identification of the causative pathogen. Indeed, delay in effective treatment reduces the survival rate on average of 8% for the each following 6-hour period [5–7]. However, extraction of pathogen agents in the range of 1–5 units per ml with clinical relevance is a critical issue. Meanwhile, the gold standard blood culture (BC) approach for pathogenic and antibiotic susceptibility identification remains yet a major limitation with turnaround time of 2–5 days [8, 9]. Moreover, less than 10% of blood samples processed from hospitalized patients with blood infections are positive [10, 11]. Decreasing the sample analysis time compared to classical methods with microfluidics thus appears very challenging for diagnosis. In this section, main sorting, extraction, and purification methods are introduced.

2.1. Passive approaches

2.1.1. Surface binding technique

Solid-phase extraction technique (SPE) is the most widely used preconcentration and purification technique. Capture is performed through a hydrophobic interaction between the analyte and a confined monolith element. Subsequently, a washing step to eliminate interference components is achieved. Finally, the elution step releases the trapped components. From cardiac biomarkers, nucleic acids to proteins, monolith materials with or without functionalization are used as the preferred on-chip approach for purification and concentration. Indeed, monoliths are intensely used, because of ease of preparation, wide ranges of formulation, and adjustable surface area and porosity. Monoliths are commonly prepared via photo-polymerization or sol-gel approaches. Recently, in a PCO microfluidic chip based on an octyl-methacrylate-based polymer monolith, Yang et al. [12] have shown that the ratio of monomer to pyrogen can be adjusted to change the porosity of the column. In addition, the system features a fluorescence labeling capability where model HSP90 proteins were labeled on-column, prior to their elution. Extending the range of suitable materials for SPE integration in an all polymer approach, Lounsbury et al. [13] developed an original PMMA-based column extraction method within a fully integrated device for the sample-to-PCR products collection. From buccal swabs to whole blood samples, they showed a ~5-fold reduction in processing time for complete amplicon purification and extraction. Beyond continuous and static monolith approaches, bead materials alternatively might be used for capture and extraction. Indeed, using silica beads, and others chitosan-coated beads among others methods, many systems have been implemented. However, some limitations may occur due to packing difficulties in such complicated designs. Using a dual-weir filtration strategy for bead immobilization, Zhong et al. [14] were able to extract and purify λDNA in a glass chip system, finally eluted in a small volume of ~8 μL. In order to circumvent the relative difficulties of bead packing, static silicon micropillars have been fabricated directly inside the microchannel. Repeatedly separated micropillars promote recombined multiple flow streams favoring DNA contact with the silica surface areas. Since extreme high flow rates can be operated (10 ml min^{-1}), this strategy appears of great interest for medical applications. Finally, the system featured a binding capacity of 57 ± 5 ng cm^{-2} [15]. For medical applications, the direct molecular concentration from a real biofluid remains a difficult issue; therefore, it might be preferred to extract a cellular group instead of a molecular species. Indeed, super-macroporous cryogels, with interlinking pores ranging from 10 to 100 μm, with added targeted ligands inside the gel trapped cells of interests [16]. In addition to blood cells, bacteria such as *Escherichia coli* have been shown to absorb over the gel.

The definitive easiness and reported performance of SPE strategy position this approach at the leading position for on-chip purification and concentration. Additionally, since two decades, numerous similar off-chip SPE and bead technologies have been developed and even been commercialized, their integration inside lab-on-a-chip (LOC) system should, therefore, benefit from those achievements. Agilent (Santa Clara, CA, USA) and Bio-Rad (Hercules, CA, USA) companies developed their 2100 Bioanalyzer and Experion™ automated electrophoresis

systems, respectively, for nucleic acids and protein analysis. These systems perform all of the steps of gel-based electrophoresis synthesis, molecular staining and final imaging.

2.1.2. Solvent extraction

As solid phase extraction, solvent phase extraction is an off-chip mature technique for separation and preconcentration of analytes. Liquid-liquid extraction (LLE) in the LOC system benefits from short molecular diffusion, low consumption and high extraction efficiency due to large specific interfacial areas. Chen et al. [17] reported a concentration factor of over 1000 for butyl-Rhodamine B using only few hundreds picoliters of organic solvents. Kitamor's group developed several glass chip extraction systems with channels ranging from 20 to 200 μm for successive extraction of Nickel and Cobalt complexes [18, 19], drugs of abuse species concentrated from urine (amphetamine, mephentermine) [20] and finally carbamate pesticides for agronomics purposes [21]. Especially for molecular microbiology, LLE is a conventional method for nucleic acid purification and extraction from lysate of various clinical isolates. Indeed, the cellular membrane components and proteins move toward the organic/aqueous interface while the DNA stays in the aqueous phase, which is then subsequently removed. Based on phenol-aqueous extraction system, Reddy and Zahn [22] performed either genomic or plasmid DNA extraction and concentration in a 30 μm deep and 80 μm wide microchannel glass chip. Several optimization strategies based on flow velocities and their profile properties for enhanced interface stability and surface modification have been proposed. Concerning microstructures and surfactants that are the most concerned parameters for extraction performance improvements, the readers could further read to the following complete review [23].

To sum up this section, regarding materials, one could clearly observe that all reported systems have been realized using either glass, silicon, or quartz interface. Straightforwardly understood, it should be noticed that with the involved organic solvent, polymer approach lack of intrinsic chemical resistance, avoiding their use in the field. But on the other side, glass bonding, typically achieved in between 350 and 650°C for several tens of minutes, induced major drawbacks (i.e., bioreagents integration and biochemical surface functionalization), heavy cost issues and limited throughputs. Dedicated efforts to implement highly chemically resistance polymers such as a Teflon-like (e.g., PFA, PEFE) or polyimide interface should be a way for significant advances of liquid-liquid extraction methodology for cost-effective LOC platforms, where additional downstream amplification and detection means with on-board reagents would be, therefore, possible to be integrated.

2.1.3. Microscale filters

Compared to SPE or liquid-liquid phase extraction methods, microscale filtration is performed in a single buffer system. Typical filtration approaches involve two large mechanisms. First, the filtering effects those permit sorting through their pores by steric exclusion. Second, electric fields that will induce transport of the analyte inside or at the vicinity of the pores sites. Only representative works based on the first steric aspect, considered as "passive approach," are addressed in this section. Exclusion/enrichment effects based on electrical fields are presented later in (Section 3.2).

Mainly four types of filtering approaches are commonly used: membrane, weir, pillars, and cross-flow. First, integration of optically clear polycarbonate track-etched membrane is one of the preferred options for membrane based filtration approach. At low cost, an impressive range of membrane features are available with thicknesses ranging from 5 to 50 μm, pores sizes from 10 nm to 10 μm, and pores density from 10 + 5 to 10 + 9 pores cm^{-2}. Additionally, such membranes can be easily integrated in a multilayered microfluidic system. In order to reduce their clogging and fouling issues specific microfluidic protocols have been investigated. Using the periodic reverse flow strategy, Redkar and Davis [24] have shown that the final average flux obtained with backflushing is still 20–30 times higher than filtration without the reserve flow strategy. Recently, in order to separate diverse multicomponents from a sample, Lo and Zahn [25] have integrated three membranes with pore size of 0.4, 2, and 5 μm in a microfluidic chip. Therefore, from one side to the other, they demonstrated the separation of sheep blood into its components. Conventional membrane filtration has been also optimized through the cross-flow approach. Recently, Aran et al. [26, 27] reported a cross-flow filtration using the track etched membrane integrated in a microchannel for the continuous bacteria extraction from whole blood for sepsis interest and also plasma protein extraction during cardiac surgery. Compared to isoporous planar membrane integration, the weir and pillar-based filtration approaches benefit of added advantages such as the flexibility of microfluidic design and microfabrication since pore size, filter orientation, and geometry can be modified on demand in order to improve microscale interaction in between filters structures and filtrate. Recently, using a weir-type filter, Chung et al. [28], developed a microfluidic cell sorter for circulating tumor cell (CTC) concentration and analysis. Moreover, the continuously separation is achieved at a high flow rate of up to 20 ml/h (see Figure 1a). Micropillar arrays for CTC isolation, fetal red blood cell enrichment and removal of pathogens have been also intensively used in microfluidic environments [29, 30, 31]. For further interest, we refer the readers to the following reviews [32, 33].

2.1.4. Hydrodynamic sorting and concentration techniques

Hydrodynamic methods that are passive approaches represent the most widely used strategies for sorting and concentrating micron-sized objects. Hydrodynamic methods rely on any external field other than the forces developed by the fluid on the analyte. These techniques not only ease the overall concerns of integration, but also feature promising potential for high-throughput and enhanced parallel purposes. Additionally, hydrodynamic techniques are label-free. Relying mainly on microscale microfluidic effects based on deterministic lateral displacement (DLD) [34], hydrodynamic focusing [35], and inertial migration mechanism [36, 37], various demonstrations have been already reported. In this section, we only report for few significant examples for each approach, for in-depth review and exhaustive hydrodynamic understanding, we refer the readers to aforementioned publications [38].

Last refinement for DLD systems focused on the optimization of the geometrical boundary of micropillar components which drive the separation performance of the system. In that sense, Inglis [39] has proposed fluidic aberrant corrections for enhanced separation characteristics. In order to reduce clogging and fluidic resistance for high DLD performance, Loutherback et

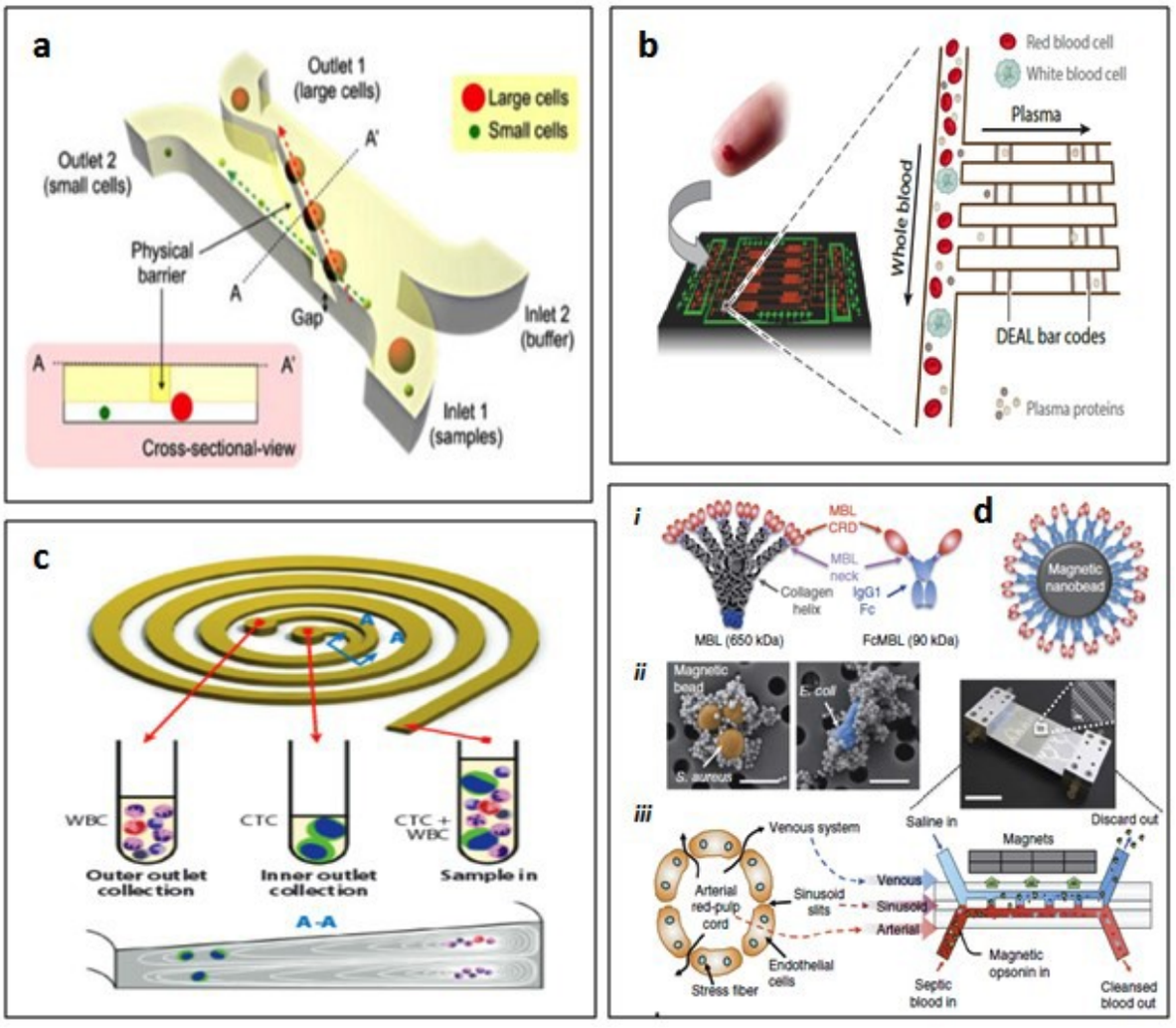

Figure 1. (a) Schematic illustration of a cross-flow microfluidic cell sorter used to separate circulating tumor cells from normal blood cells. Large cancer cells move along the weir-type barrier and are collected at one outlet while smaller hematological cells pass through a gap underneath the barrier, and are directed to a separate outlet. (b) An integrated blood barcode chip for a protein assay. Plasma is separated from blood collected from a fingerprick by harnessing the Zweifach-Fung effect. Proteins in plasma are skimmed and analyzed *in situ* within the antibody barcode arrays. (c) Schematic of particle separation using a spiral microchannel with a trapezoidal cross-section. At the outlet of the spiral microchannel (the A-A cross-section), CTCs are focused near the inner wall due to the combination of inertial lift force and Dean drag force at the outlet; white blood cells (WBCs) and platelets are trapped inside the core of the Dean vortex, which is formed closer to the outer wall. (d) (i) Magnetic opsonin and biospleen device. Design scheme of native mannose-binding lectin (MBL) to produce the generic opsonin FcMBL and its coating on magnetic nanobeads to ensure stable and to facilitate protein purification. (ii) Pseudocolored scanning electron micrographs showing magnetic beads (128 nm) bound to the bacteria *S. aureus* (orange/brown; left) and *E. coli* (blue; right). Scale bars, 1 μm; arrows indicate pathogen with bound beads. (iii) Schematics of a venous sinus in the red pulp of the spleen (left) and a longitudinal view of the biospleen (right), with a photograph of an engineered device (right).

al. [40] have integrated several pillar structures (circular vs. triangular) and their gaps. Finally, combining those two corrections, 85% of CTC recovery was achieved operating at an impressive flow rate of 10 ml/min [41]. *E. coli* and trypanosomes pathogenic cell extraction by DLD have been reported using circular posts of 6 and 20 μm, respectively [42, 43].

http://dx.doi.org/10.5772/65772

Hydrodynamic focusing refers to the use of flow streams to achieve cell or bead concentration and isolation. It is a size-based approach controlled by the flow rates, channel geometry and downstream channel configurations. For continuous plasma extraction, Vermesh et al. [44], developed an integrated blood bar code system displaying two units. First acted for plasma microfluidic skimming, when the size of the cells are comparable to a main central channel width the cells at a bifurcation point migrate toward this high flow rate channel while plasma penetrates adjacent perpendicular channels. The harvested proteins can then react on probes deposited inside the adjacent channels as illustrated in Figure 1(b).

Finally, due to its improved performance when operating at high flows, inertial focusing in recent years has gained tremendous interest for diagnostics, therapeutics and cell applications. Related to the combined effects of the two size-dependent forces, the inertial lift force ($FL \propto a4$), and when operating in a curved channel, the additional Dean drag force ($FD \propto a$), diverse lateral positions across the channel section will be favored for specific particle geometry for sorting and concentration purposes [45]. In a recent study, using optimized spiral devices with trapezoidal cross-section, a recovery of 80% of CTC from 7.5 ml of whole blood have been reported in 8 min (Figure 1c) [46]. Using a combination of hydrodynamics and inertial focusing methods, Clime et al. [47] recently, devised a system for the concentration, and the cleaning of a wide range of pathogenic agents from a ground beef sample. The enrichment strategies and numerous alternatives related to the use of both microfilter and hydrodynamic methods close the loop for the concentration and sorting of micron-sized objects (cells, coupling microparticles to nucleic acids, proteins, etc.). Therefore, it is subsequently possible to reach molecular extraction and eventual higher concentration with the help of aforementioned SPE and LLE means.

In a natural manner too, those considerations might be extended to the use of magnetic labeled approaches where nanoparticles and microbeads can be implemented for enhanced sorting and concentration in combination with the aforementioned tools. However, such topics are not covered in this section. But as a unique example, we wish to report a microfluidic extracorporeal blood-cleansing device recently published in the Nature Medicine Journal [48], where therapy has been used for large spectrum of pathogen and toxin removal from blood. The capture was performed with magnetic nanobeads coated with human mannose-binding lectin under the application of an external magnet through a micron-sized nanoporous membrane, which pull the opsonin-bound pathogens and toxins out from the blood. The system was operated at a tremendous throughput up to 1.25 l/h in an *in vitro* approach and the extraction performance cleared more than 90% of bacteria out stream (Figure 1d).

2.2. Electrophoretic separation and preconcentration on-a-microchip

The first experimental examples of μTAS have been published in the 1990s. Whereas the conventional separation systems are based on chromatographic methods, the separation on-a-chip most often relies on electromigration methods and particularly with free zone electrophoresis [49–51]. The conventional chromatographic systems are generally considered to be more robust and reliable for quality control or medical purposes. However, the miniaturization of analytical systems has shown that electrophoresis on a chip is a versatile analytical separa-

tion technique that may provide high separation efficiency. Manz et al. [52] have pioneered the electrophoretic separation of sample mixtures in glass microchips. Their work that is one of the most cited papers has demonstrated the ability of a simple chip with optical detection to separate several amino acids in 15 s. The electrophoretic and electroosmotic mobility are the two contributions of transport in electrophoresis:

$$v = \left(\mu_e + \mu_{eof}\right) \tag{1}$$

where v is the migration velocity of the analyte, μ_{eof} is the electroosmotic mobility and E is the electric field.

Compared to the parabolic profile with Poiseuille flow obtained for chromatographic techniques, electrophoresis in a microchannel produces a plug-like flow with more homogenous distribution of the velocity vectors. Thus, the electrophoretic profile presents sharp peak and it helps to improve the analytical resolution. The surface to volume ratio is rather high in microfluidics and the electroosmotic mobility expression renders electrophoresis very sensitive to the surface state of the inner wall of the microfluidic channels. From this assessment, we could think that the modulation of surface charge is one way to improve the robustness of analytical performances of electrophoresis-based separation on-a-chip. The resolution in this kind of separation is also directly linked to the electroosmotic mobility by the following equation [53]:

$$R = \frac{1}{4(2)^{\frac{1}{2}}}\left(\mu_{e1} - \mu_{e2}\right)\left[\frac{E}{D\left(\overline{\mu_e} + \mu_{eof}\right)}\right]^{1/2} \tag{2}$$

where μ_{e1} and μ_{e2} are, respectively, the electrophoretic mobilities of two different analytes and upper lined μ_{e} is the mean electrophoretic mobility, and D is the diffusion coefficient.

By considering Eq. (2), if the mean electrophoretic mobility and the electroosmotic mobility have opposite sign and similar absolute values the resolution parameter R is maximized. Various strategies have been published in the literature to adjust the surface charge and thus the electroosmotic mobility. The simplest way to tune this parameter is to perform surface treatment with polymers, self-assembled monolayers by adding organic solvents in the buffer [54].

Another strategy consists of integrating a fluidic transistor in the separation channel. The gate voltage of the fluidic transistor will modify the surface state in a more versatile manner. Van den Berg et al. [55] pioneered the introduction of insulated electrodes in the separation microchannel. The electrode and the upper insulating layer interact with the ionic species of the liquid/solid interface to adjust the surface charge. This first microfluidic transistor has shown its ability to drastically change the zeta potential. This microfluidic device is capable of adjusting the electroosmotic mobility and even choosing the direction of its vector. This

http://dx.doi.org/10.5772/65772

dynamic control of electroosmotic flow (EOF) requires a calibration of the gate voltage versus the electroosmotic mobility in the chosen buffer.

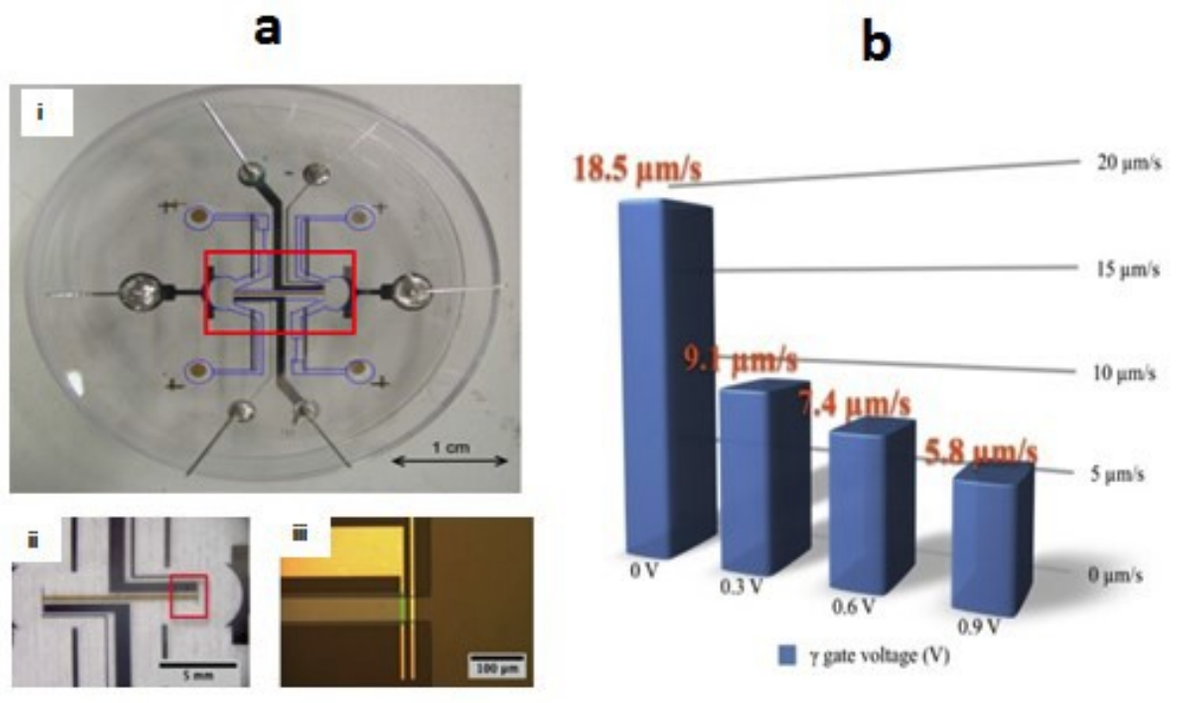

Figure 2. (a) Photography of the Wheatstone fluidic bridge bearing a fluidic transistor in the middle. The blue dashed lines are showing the fluidic network of the device. A zoom of the red box of the (i) photography is given in (ii). This optical microscopy image shows the three pairs of electrodes in the central microchannel. The brown scheme of the central channel bearing a fluidic field effect transistor. Again a zoom of the red window of the B image is proposed in (ii). In this latest image we distinguish the reference electrode of the right part of the fluidic transistor. The gate electrode (green) is placed between the ITO adhesion layer and the SiC polarizable layer. (b) Velocities of the fluorescent microbeads measured from the PIV image analysis as function of the gate voltage of the fluidic transistor. Electrophoresis in the central channel is still 3.33 V/cm.

In Haghiri's group, a new generation of fluidic field effect transistor (FFET) with a direct contact between a polarizable electrode and the buffer has been proposed and studied since 2007 [56]. This fluidic component requires less voltage to adjust the surface charge and avoids the problem of current leakage from the insulating layer that is observed during ageing with the Van den Berg's transistor. On the other side, the polarizable interface will be more sensitive to unspecific adsorption or any surface contaminations. Our first attempt to adjust the surface charge with such polarizable interface was already published and we partially succeeded to control the zeta potential with three different materials. With the first generation of FFETs, some electrochemical reactions have been observed, leading to the partial destruction of the transistor. Moreover, the linear variation of the electroosmotic mobility versus the gate voltage could be surprising since the equivalent electrical model includes a capacitance. For the second generation of FFETs to avoid these parasitic electrochemical reactions, the gate voltage of the polarizable interface should be adjusted from a reference electrode close to the transistor. In

addition, voltage followers have been integrated in the electric system of the transistor. The electric potential of two reference electrodes at both side of the transistor could thus be connected to these voltage followers to precisely adjust the gate voltage. Moreover, the SiC polarizable interface does not directly adhere onto the glass surface since a layer of ITO (indium titanium oxide) between the substrate and the polarizable layer allows to electrically isolate the SiC polarizable interface. This configuration of flow field effect transistor was integrated in the Wheatstone fluidic bridge to measure the EOF mobility as a function of time. Compared to the first generation FFET transistor without reference electrodes a drastic decrease of the electrochemical reaction was observed. A microfabrication process including WL-5150 photosensitive resist and metal deposition onto glass substrates was optimized. The inlets and outlets of the device are opened by gently sandblasting the upper glass substrate. The total thickness of the double ITO/SiC layer is 200 nm. Pictures of the Wheatstone fluidic bridge with a transistor are given in Figure 2(a). The fluidic flow in the central channel is controlled by the modulation of the EOF flow and thus can be adjusted by the value of the gate voltage. A 5 V transverse electric field was applied with the extreme electrodes for electrophoresis. The gate voltage values were less than 1 V in the polarizable window of the SiC. Particle image velocimetry (PIV) was used to characterize the fluidic flow as a function of the gate voltage. Indeed, 1 μm diameter fluorescent bead was injected in an aqueous 10^{-3} mol/l KCl solution. Finally, the modulation of the fluidic flow as function of the gate voltage is shown in Figure 2(b). It should be noticeable that the amplitude of the velocity is decreased by more than a factor three between a gate voltage of 0.9 and 0 V. The gate voltages used in these experiments are very low compared to values used in the MIE (metal-insulator-electrolyte) configuration (few hundreds Volts).

The development of electrophoresis on-a-chip has led to high-throughput microfabrication methods to produce cost-effective miniaturized fluidic devices. Recently, Liedert et al. [57] reported a foil-based PMMA chips fabricated by high-throughput roll-to-roll (R2R) process for the identification of the antibiotic resistance gene *mecA* in *Staphylococcus epidermidis*.

Pu et al. [58] pioneered molecular enrichment using nanofluidic devices. Electropreconcentration with nanoslit is used to rapidly and locally increase the concentration of low abundant species. The group of Santiago [59], leader in the field, performed most efficient and innovative ways to preconcentrate several analytes and address the most significant theoretical concerns. However, the influence of several parameters such as ionic strength, chemical nature of the buffer or the surface charge of the inner walls of the device is not yet fully understood and there is still a need for pertinent preconcentration diagrams. The micro-nano-microstructure and real pictures of the electropreconcentration chip are presented in Figure 3(a) [60]. Moreover, we add in this figure the velocity profiles by considering the electrophoretic and the electroosmotic contributions and the influence of an additional hydrodynamic pressure. This additional pressure permits modification of the position of the preconcentration plug and even stabilizes some propagating regimes. Moreover, such hydrodynamic pressure stabilizes the concentration polarization effect and controls the selective preconcentration of analytes in terms of preconcentration rate and localization as compared to pure electrical preconcentration (see Figure 3b).

http://dx.doi.org/10.5772/65772

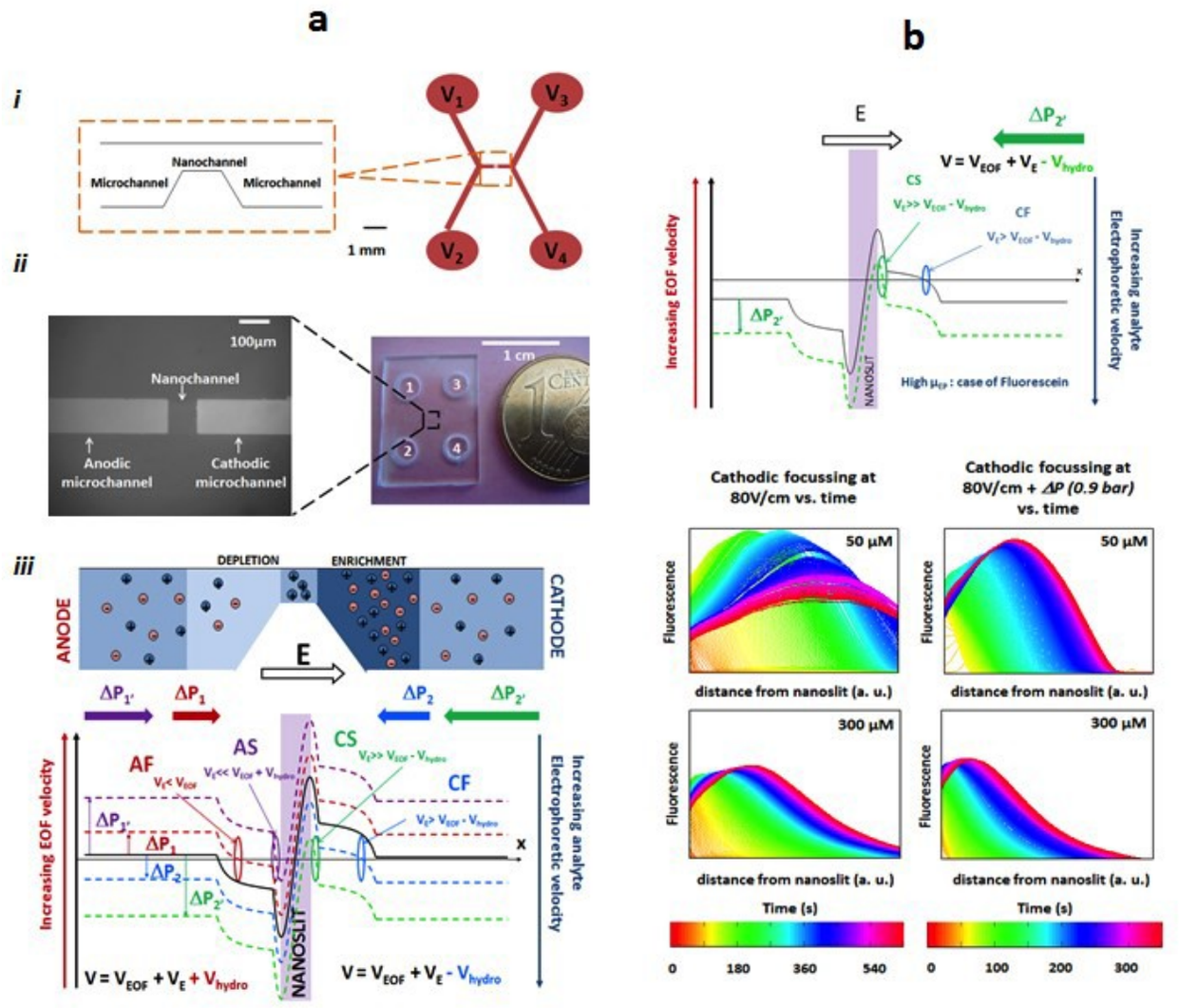

Figure 3. (a) (i) Scheme of the central channel of the preconcentration device. The nanoslit is connected by two microchannels to obtain the microchannel/nanoslit/microchannel structure (MNM). (ii) Microscopy picture of the MNM structure during an electropreconcentration experiment. The fluorescent analytes are injected at both sides of the device. On the right we show a photography of the whole preconcentration device. (iii) The mechanism of pressure-assisted preconcentration and separation. The local transport rate profile is represented in the MNM structure (velocity of the molecule vs. distance in the structure). The black curve gives the classical preconcentration global velocity of BSA when an electric field is applied as a function of the distance. Four other cases are depicted: two cases with the application of a positive pressure (from the anode to the cathode), which has the effect of moving up the curve in the diagram and obtaining the two anodic regimes depending on the value of the pressure (anodic stacking in purple and anodic focusing in red), two cases with the application of a negative pressure (from the cathode to the anode), which has the effect of moving down the curve and obtaining the two cathodic regimes (cathodic stacking in green and cathodic focusing in blue). (b) Experiments with fluorescein show the role of the ionic strength and the addition of a hydrodynamic pressure over the evolution of the preconcentration profiles (left) a conventional electropreconcentration compared to (right) a cathodic-pressure-assisted electropreconcentration [60].

3. Detection components and microfluidic strategy

3.1. Introduction to MEMS detection

This section focuses on miniaturized sensors designed for getting, which are integrated in the last stage of the fluidic lab-on-a-chip (LOC) device after preconcentration and separation previously discussed. Integrated microfluidic biosensors can be classified into two main categories: (1) bulk detection**,** more often named labeled detection allowing identification of analytes flowing inside the fluidic channel with prelabeling of the target with a marker (fluorescent or electroactive marker) and (2) "label-free" detection, where physical effects during biochemical recognition are directly measured after binding of the target analyte on the chemical probe. More often this detection mode occurs on a surface, which has been functionalized with the bioreceptor (probe) [61]. Figure 4(a) illustrates these two routes for a classical "Primary antibody/Antigen" couple. The biochemical recognition is mainly governed by the choice of the appropriate biochemical receptor that will specifically bind to the target of interest. Receptors are thus integrated in architectures specifically designed to be well adapted for both analyte and transduction method. Figure 4(b) presents the different existing architectures [2]. In brief, transducers have been paired with antibodies (or antibody fragments, i.e., proteins that are produced by the immune system) [62, 63] see Figure 4(b) (i), with aptamers [64] (see Figure 4b(ii)) and other receptors as recognition elements (Figures 4b(iii)–(v)). For surface detection, if the affinity of the biomolecular recognition is high ($K_a = k_{on}/k_{off}$ ranging from 10^9 up to 10^{13} for the case of biotin and streptavidin), the identification of the target can be highly selective during its capture by the bioreceptor. If the specificity of the biochemical recognition is fully determined by the nature of bioreceptor, the sensitivity, also called "Limit-of-Detection" (LoD) and the dynamic range of the sensor are strongly related to the intrinsic properties of the transducer.

It is thus of interest to review different intrinsic properties of the transduction, which can be mechanical, magnetic, optical, or electrical (Figure 5) [65–71]. They are very few comparative studies on intrinsic sensitivity in the literature. However, the reader could refer to the excellent review paper of Arlett et al. [73] published in Nature in 2011, which summarizes and compares the performance of mechanical, optical, and electrical transduction methods. Mechanical sensors are based on cantilever assays where the specific binding of analytes induces lateral stress, resulting in bending of the free-end of the cantilever. One major limitation of surface cantilever detection (Figure 5b) concerns nonspecific binding occurring at the bottom cantilever surface that can negate the bending and thus alter the detection. Recently, Ndieyira et al. [66] have shown that it is possible to overcome competing stresses from opposing cantilever surfaces allowing direct capture of HIV molecules at 500 fM within 15 min. Magnetic sensors have been mainly used to manipulate magnetic beads in fluidic channels that are used as magnetic label for cell sorting or bead detection [67]. We do not detail such sensors in this chapter since extensive reviews exist. The reader can refer to the excellent reviews from Pamme and Gijs that give a general overview of magnetic integrated sensors [74, 67]. The last part of this chapter is devoted to intrinsic performances of both optical and electrochemical biosensors

http://dx.doi.org/10.5772/65772

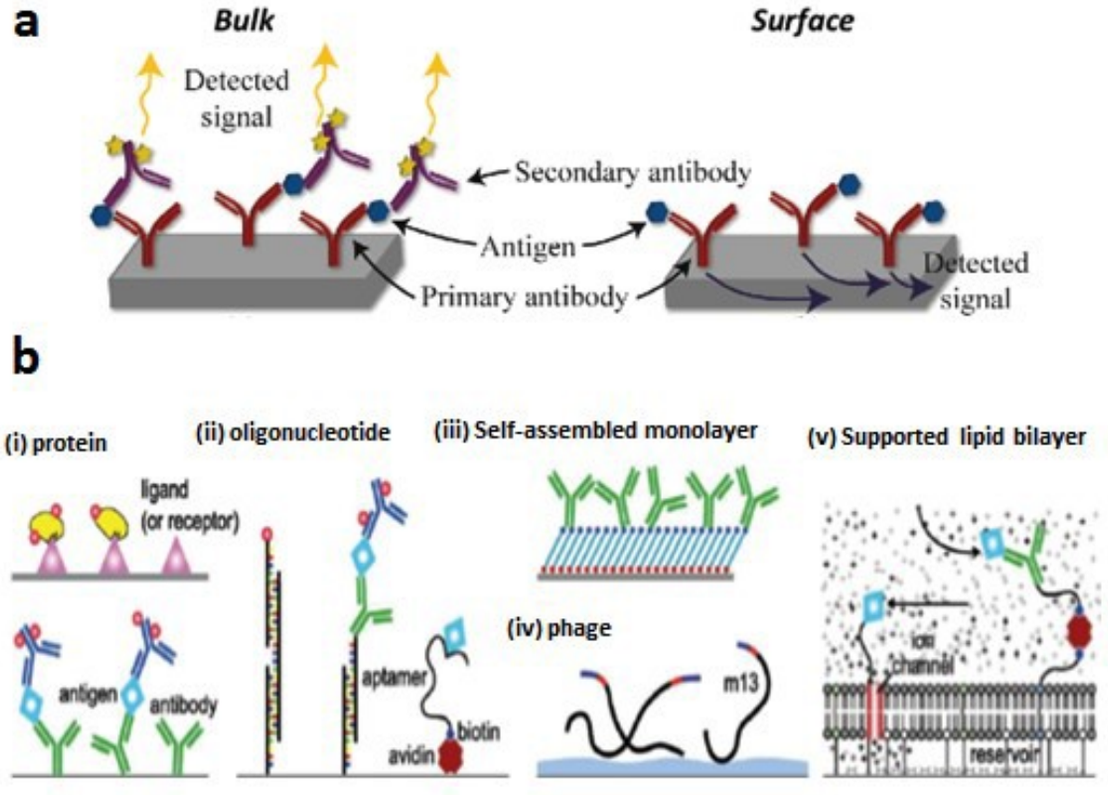

Figure 4. Comparison between (a) labeled and (b) label-free detection methods, reprinted from [61], examples of the different architectures for surface functionalization, reprinted from [2].

and, finally, we conclude with recommendations for optimizing fluidic parameters in order to enhance the capture of biomolecules.

3.2. Optical and photonic detection

In general optical biosensors are divided in fluorescence-based and label-free detection. In fluorescent-based detection (bulk), the evanescent field is used to enhance the excitation (or the emission) of the fluorescent dye used to tag the analyte of interest. In contrast, in label-free detection, the target molecules are not labeled and are detected in their natural forms. Optical sensing remains an important route for which record sensitivities were demonstrated through the considerable progress of photonic nanostructures. We focus in this section on integrated photonics nanosensors that are based on direct coupling between light and fluid since the strength of this interaction determines the intrinsic sensitivity [75]. Before, discussing the specific properties of the different photonic sensors, it is of interest to illustrate how such photonic nanostructures could be integrated inside the microfluidic chip.

The optofluidics device thus integrating source and detector exhibits new optical properties related to the nature of liquids. This concept of optofluidics multilevel platform has been introduced by Psaltis at the University of Caltech in the Unite States [76]. In such platform three levels are stacked: (1) the base of the device (bottom layer) that contains the optical

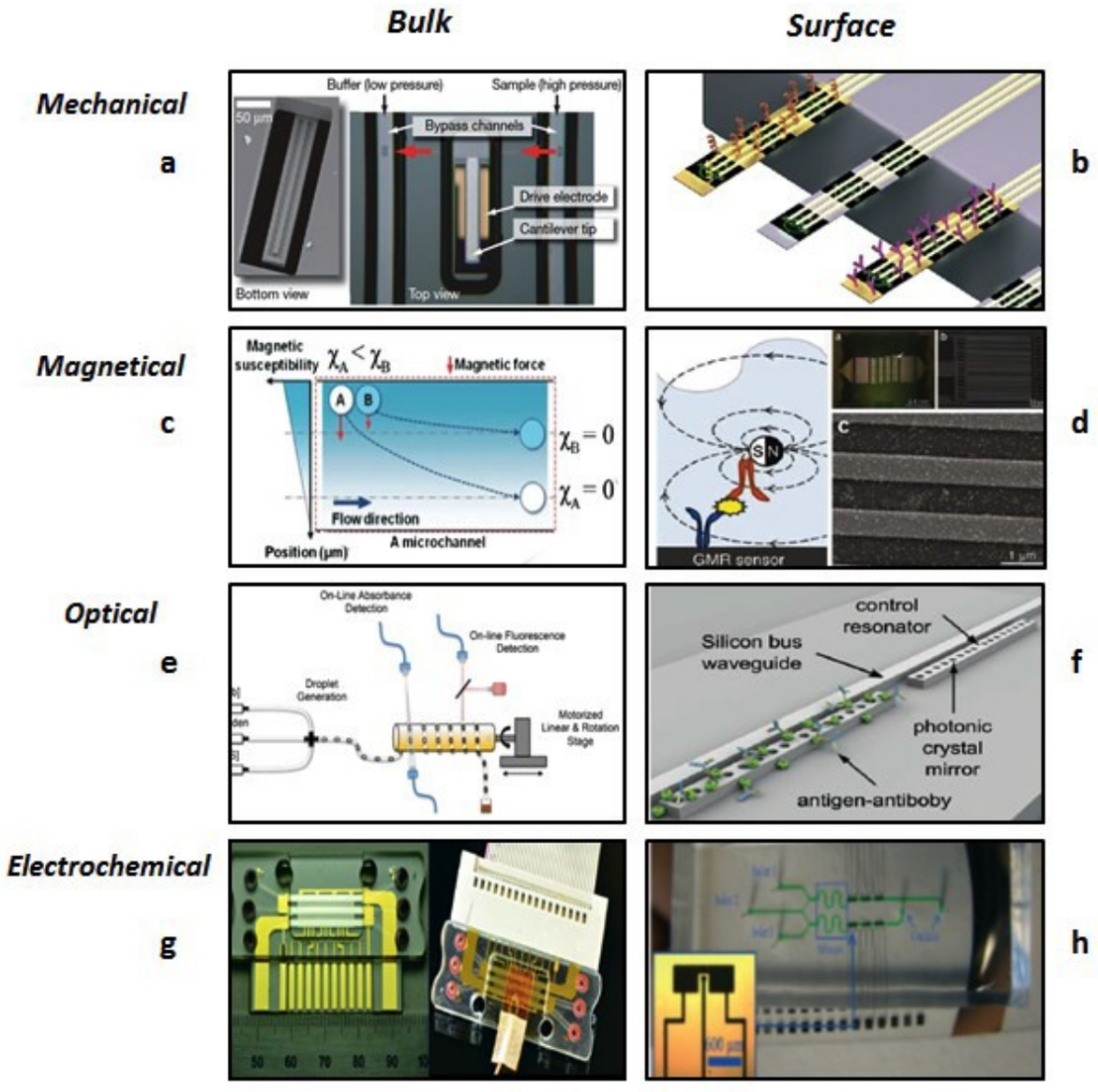

Figure 5. Examples of integrated biosensors presented as function of the nature of the transduction for both bulk and surface routes, reprinted from (a) [65] and (b) [66], (c) [67] and (d) [68]; (e) [69] and (f) [70]; (g) [71], and (h) [72].

elements, namely, the springs, the waveguides and the optical sensors (photonic-crystal or plasmonic nanostructures), (2) the intermediate layer that includes the fluidic microchannels for the circulation of biological fluid, and (3) the top layer that contains the actuators for liquid handling, i.e., valves and pumps. Figure 6 presents the hypothetical architecture of such ideal optofluidic platform based on photonic nanostructure as sensor [75, 77]. If the optical sensors are structured in the bottom layer to dimensions smaller than the wavelength of the order of 100 nm, the fluidic channels have, in turn, typical widths of hundreds of micrometers and lengths of several millimeters. There are still very few complete demonstration platforms, which integrates all the optical components (source, waveguides, and detectors) and fluid control tools. All current researches converge toward this ultimate goal of integration, hoping to increase the portability of the chip and the sensitivity of optical detectors.

http://dx.doi.org/10.5772/65772

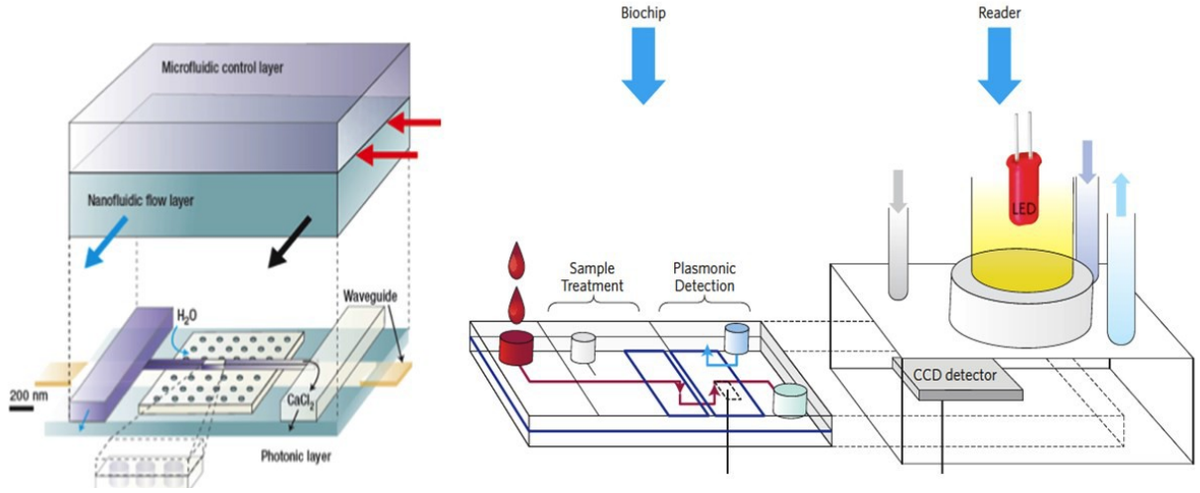

Figure 6. Hypothetical architectures for integration of photonic nanostructures with a cross-section of the fluidic chamber containing the sensor (left) and a global view of both chip and reader (right), from references [75, 77].

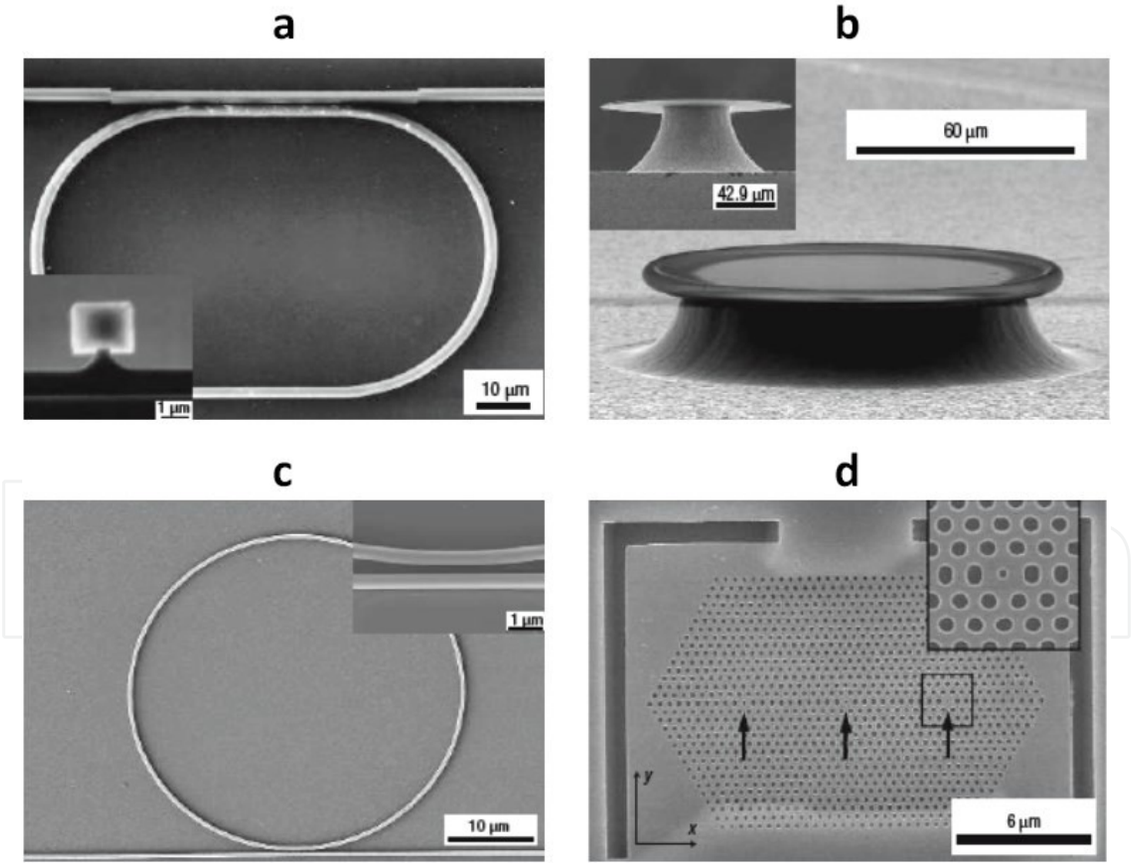

Figure 7. Scanning electron micrograph of various microcavities that can be used for biosensing with (a) suspended polymer microring from [79], (b) silica suspended microdisk (inset) from [80] and silica microtoroid from [81], (c) silicon microring from [82], and (d) planar photonic crystal in an InGaAsP membrane from [83].

In an optical biosensor the strength of light-matter interaction is enhanced by the presence of a guided or a localized optical mode with an evanescent field with subwavelength spatial extension [84, 85]. Guided mode can be excited in dielectric or metallic waveguide. A typical example is the case of the surface plasmon resonances (SPR) [80], an electromagnetic guided mode excited at the interface between a noble metal and a dielectric. Localized modes can be excited in dielectric structures like photonic crystals [86, 87] (Figure 7d) or ring resonators [79, 82] (Figure 7a and c) and in metallic nanoantenna resulting in the so-called localized surface plasmon resonance (LSPR) (Figure 7d) [83].

The light confinement can be used to increase the scattering (or the absorption) cross-section of the analyte molecules or to measure the refractive index (RI) change induced by molecular interactions. The most studied example of the first category is surface-enhanced Raman spectroscopy (SERS). SERS is a spectroscopic technique in which the inelastic scattering of monochromatic light provides information about vibrational, rotational, and other low frequency transitions in molecules of the analyte. Here, we limit the scope of this section to the so-called RI-based label-free detection. The presence of the analyte immobilized on the sensor surface through a specific biochemical reaction results in a RI change in the near field region of the optical mode. The RI change induces a modification of the dispersion relation of the guided mode or a shift in the position of the localized resonance that is monitored in real time. The performance of an RI-based optical sensor is most commonly characterized through the bulk sensitivity $S = \Delta\lambda/\Delta n$ [nm/RIU (Refractive Index Unit)] in which λ is the resonance wavelength of the optical mode and n is the refractive index of the medium probed by the near-field of the optical mode. Since it is easier to detect a given resonance shift for narrow lines, the figure of merit FOM = S/FWHM (where FWHM is the full width at half-maximum of the resonance) is a more meaningful measure of the performance of the sensor. An important parameter that is difficult to quantify is the extension of the evanescent field of the optical mode. In an optical biosensor, the analyte (with RI ~ 1.5) is specifically immobilized at the sensor surface, where the intensity of the evanescent field is higher. The rest of the evanescent field probes the RI of the buffer solution (RI ~ 1.33). The effective RI change probed by the whole near field of the optical mode depends on the overlap between the evanescent electromagnetic field and the analyte. Highly confined modes are therefore more sensitive to small analytes. This explains why, despite their relative high sensitivity and FOM (typically 3300 nm/RIU and 50), SPR-based biosensors fail to detect small molecules like biotin because of the relatively large extension of their evanescent field that exponentially decays over 200–300 nm away from the surface. On the other side, LSPR-based biosensors have relatively smaller sensitivity and FOM (typically 400 nm/RIU and 2), but their evanescent field exponentially decays over a distance 10 times smaller than that of a SPR mode [88, 89].

To our knowledge the highest FOM and field confinement achieved to date for a localized optical mode was reported by Cattoni et al. [90] in arrays of plasmonic nanocavities fabricated by soft UV nanoimprint lithography (Figure 8). The plasmonic nanocavity is designed and ensures total absorption of light at the plasmonic resonance. Sensitivity, FOM, and optical field confinement are parameters that strictly depend on the physics behind the nanophotonic element used as a sensor. These parameters alone cannot be related to the biosensor perform-

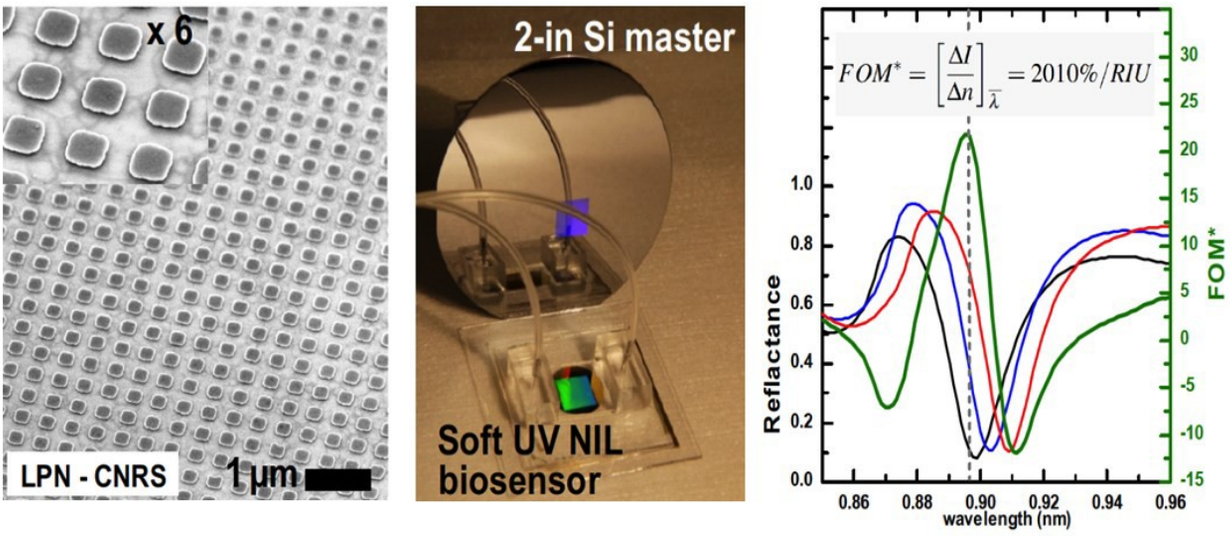

Figure 8. Left: SEM image of the 2D metal-insulator-metal nanocavities fabricated by Soft UV NIL using a hard-PDMS/PDMS stamp. Center: picture of the biosensor integrated in a microfluidic chamber and silicon master mold used to fabricate the hard-PDMS/PDMS stamp. Right: Spectral shift of the second-order mode for different RI solutions: water (black line), ethanol-water solution (blue line), and pure ethanol (red line). The green line corresponds to the FOM calculated as function of the wavelength using the equation in the inset, from [90].

ance, since it is only an indication of signal strength. The parameter typically used to characterize the performance of a biosensor is the LOD. The LOD can be deduced by taking into account the noise in the transduction signal, σ, i.e., the minimum resolvable signal: LOD = σ/S, where S is the sensitivity. The LOD can therefore be improved by increasing the sensitivity (and the light confinement) and by reducing the noise level. For an optical RI-based label-free sensor, there are typically three ways to specify LOD: in units of refractive index units (RIU), in surface mass density of the analyte (pg/mm) or in analyte concentration (ng/mL or molarity). The LOD specified in terms of RIU is easy to measure and useful to roughly compare the sensing performances of different optical sensor.

As previously mentioned, it does not take into account the extension of the field confinement because the measure is made varying the RI over the whole extension of the probing near field. Reported values for SPR-based sensor have LOD up to 10^{-8} RIU, dielectric waveguide and ring resonator LOD up to 10^{-7} RIU and photonic crystals LOD up to 10^{-5} RIU [87, 89]. The extension of the field confinement is taken into account when the detection limit is specified in terms of surface mass density, which is what a biosensor actually measures. LOD in terms of surface mass density is difficult to determine accurately, but it can be used to compare more precisely the performance of different optical sensors. Finally, LOD defined in terms of sample concentration is easy to determine and it can be used to compare more precisely the sensor performance. Of course it depends on the specific analyte and its affinity to the biorecognition molecule grafted to the biosensor surface. For this reason, LOD, chemical affinity between a specific analyte and the relative bioreceptors and microfluidic parameters must be considered all together in the optimization of the overall performances of the sensor. Acĭmovic et al. [91] demonstrated state-of-the-art paralleled LSPR-based lab-on-a-chip composed with 32 sensing

sites distributed across eight independent microfluidic channels with very high reproducibility/repeatability (Figure 9). In particular they demonstrated the fast detection of relevant cancer biomarkers (human alpha-feto-protein and prostate specific antigen) down to concentrations of 500 pg/ml in a complex matrix consisting of 50% human serum.

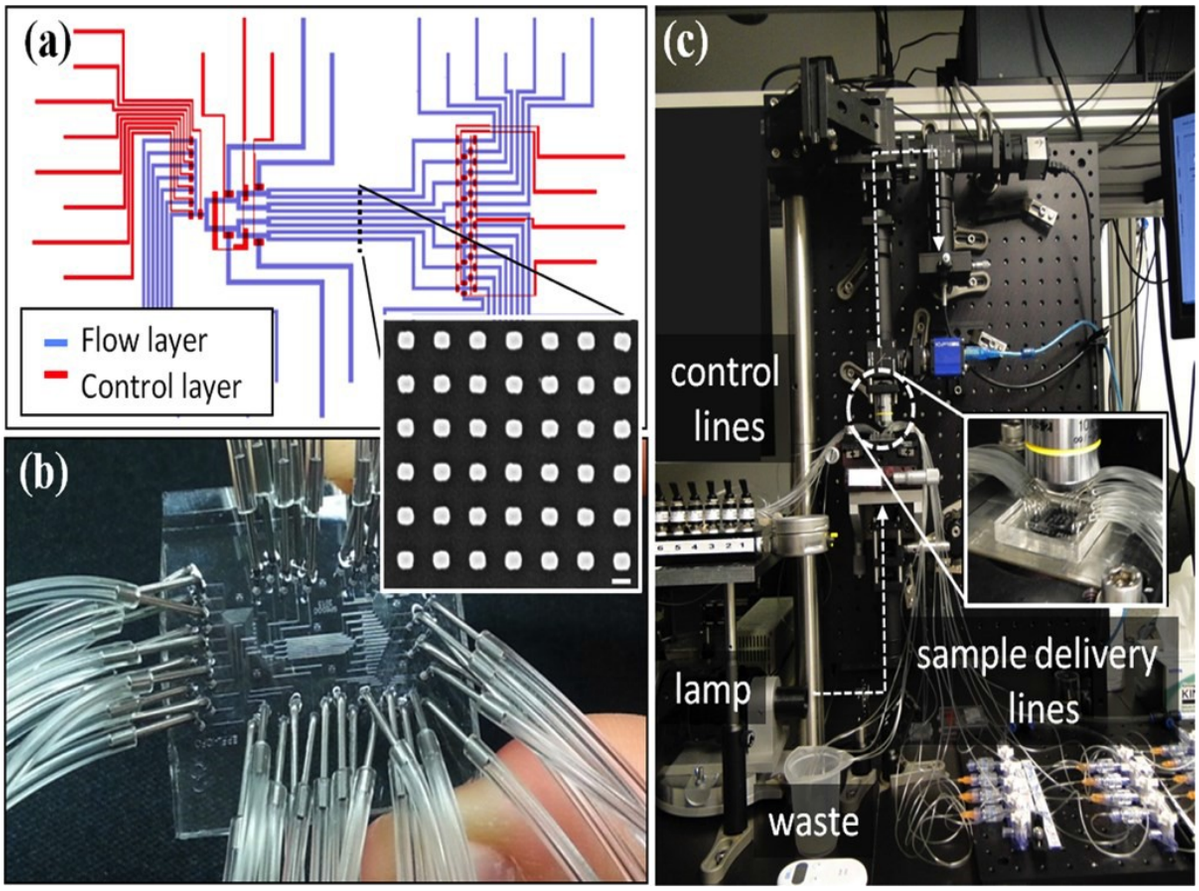

Figure 9. Description of the sensing platform: schematic of the flow and control layers (a) and final connected chip. (b) The inset shows a standard SEM image of the plasmonic gold sensors. Scale bar = 200 nm. (c) Overview of the optical setup. From [91].

3.3. Electrochemical detection

3.3.1. Introduction to microfluidic detection

Initially sensing research focused mainly on the performances of the transducer and the biomolecular recognition, without discussing the role of microfluidic parameters. To obtain a well performing analytical device these components have to be considered all together in the optimization of the overall performances of the sensor. Achieving fast time less than one minute, specific and sensitive detection at concentration on the femtomolar level or even less appear thus an actual challenge for the microfluidic community. If the main advantage of microfluidic devices is to reduce the volume and to efficiently deliver target molecules to the sensor surface, working with such extremely reduced size and concentration raises funda-

mental questions about physical and chemical limits. Independent of the intrinsic sensibility of the sensor (optical or electrochemical), all the fluidic conditions have to be chosen in order to favor binding mechanisms. For most of applications, if the fluidic system works under "extreme fast" flow at a high Péclet number (Pe_H), the number of captured molecules per unit of time is largely enhanced (see Box 1 that resumes the pertinent fluidic parameters). The geometry of the fluidic channel (the height H and the width Wc), the size of the sensor (the width Ws and the length L) and the volumetric flow rate Q have thus to be precisely defined to fix if the system will work in a reaction-limited or diffusion-limited regime.

Box 1 – Kinetics and mass-transport in microfluidics devices

To determine in microfluidic devices whether analytes are depleted in the vicinity of the sensor surface and which limiting factor governs kinetics, several parameters have to be considered.

First, the two Péclet numbers, $Pe_H = Q/D \times W_c$ with subscript H to specify the channel height as the relevant parameter and $Pe_s = 6\,(L/H)^2 Pe_H$, where D is the diffusion rate, Q is the volumetric flow rate, W_c is the channel width and L is the sensor length. Let us consider the case of a microscale sensor with $L = 50\ \mu m$ and $W_S = 50\ \mu m$ integrated in a microfluidic channel with $H = W_c = 100\ \mu m$, through which a target solution with diffusivity $D = 10\ \mu m^2/s$ flows at a flow rate $Q = 10\ \mu l/min$. Such microfluidic system exhibits large values of both Peclet numbers: $Pe_H = 1.7 \times 10^5$ and $Pe_s = 2.5 \times 10^7$ which means that the depletion zone is thinner than the channel and the sensor:

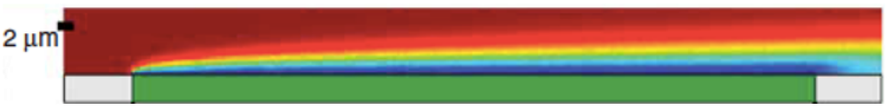

$$\delta_S \sim L_S/(Pe_s)^{1/3} = 800\ nm \ \ll L < H$$

The total flux or collection rate of target molecules can also be deduced from $J_D = Dc_0 W_S F$ where c_0 is the initial concentration of the target and $F \approx 0.81\ Pe_s^{1/3}$ the dimensionless mass transport flux: $J_D = 0.15$ molecules per second or one binding event every 7 s. In other words, a high number of targets can be trapped in the thin depletion layer where they can reach rapidly the sensor surface to fast stick on the probe and react. Working under high flow with microscale integrated sensors allows trapping sufficient molecules even in extremely diluted solutions. See ref. [92] for more details.

In 2008, Squires, Messinger and Manalis proposed a theoretical approach to estimate the interplay between diffusion, convection, and reaction [92]. Their complete analysis gives some guidelines to estimate some fundamental quantities, such as fluxes, collection rates, and equilibration times. Based on dimensionless parameters that are straightforward to compute, their simple approach is very useful in characterizing and designing systems. Two Péclet numbers, Pe_H and $Pe_{S,}$ characterize the nature of the mass-transport depletion zone around the sensor. At low values of Pe_H ($Pe_{H \ll 1}$ at extremely slow flow), the system is in a diffusive regime, with a depletion zone that extends far upstream in the whole thickness of the channel. Even if all molecules are collected, the time of capture is so high (hours or days) that such diffusive regime appears very limited for real applications. At high Pe_H ($Pe_H \gg 1$ at extremely fast flow), a depletion zone thinner than the channel (δ_S) exists and a second pertinent Péclet number Pe_S can be used to calculate whether this depletion is thicker or thinner than the sensor itself. Box 1 gives the more important equations useful for optimizing integrated microfluidic devices that involve very small volumes of sample. One should ensure that the sensor exhibits enough

sites to bind target molecules maximally. It appears that the sensor should be preferably microstructured with dimensions ranging from 100 μm to several hundreds of microns instead of tens of nanometers as for nanowires.

3.3.2. Current status and state-of-the-art of electrochemical detection

The need for a miniaturized sensor, portable, with fewer components has allowed the development of electric sensors (chemical or biochemical) [93]. Successful integration of microelectrodes opens the way for the development of electrical and electrochemical detection in microsystems. Indeed, the development of microfabrication techniques to produce microelectrodes was decisive for bioelectroanalysis. The advantage of making electrical transducer sensors is to have portable electrical and electrochemical sensors with easy operation, a great performance in the detection and a low power consumption (applied and measured signals require only a voltage generator). In addition, it contains few components on the very small dimension reducing drastically the size of the final microsystem [94]. In general, electrical sensors operate an electrical signal (current or potential) by amperometry, voltammetry [95, 96], or electrochemical impedance spectroscopy [97]. Electrochemical strategy has been used over a wide range of biochemical identification and analysis purposes from traditional genomics and proteomics areas but it find through cellomics and gases detection increasing interests. For traditional, micro-array DNA electrochemical detection, many works have been reported, and even additional on-board components such as cellular lysis, and genomic preamplification been also incorporated. Indeed, Ferguson et al. [98] have demonstrated the integration of loop-mediated isothermal amplification (LAMP) means coupled with a sequence-specific electrochemical detection in a disposable, monolithic chip. Using this platform, the authors have demonstrated detection of genomic DNA from *Salmonella enterica serovar Typhimurium* LT2 with a limit of detection of 10 aM. On the proteomics side, a recent paper from O. Kelley et al. [99], demonstrated clinical relevance for an electrochemical enzyme-linked immunosorbent assay for HIV antibodies identification. The current method derived from the oxidation increased linearly over a wide antibody concentration range (0.001–1 μg. ml^{-1}), with a detection limit of 1 ng. ml^{-1} (6.7 pM). For cellomics purposes, Zór et al. [100] recently, demonstrated a powerful electrochemical based integrated platform for real-time monitoring of cellular dynamics. Their system performed, the complete cell based assays comprising online electrode cleaning, sterilization, surface functionalization, cell seeding, cultivation, and electrochemical real-time monitoring of cellular dynamics. To demonstrate the versatility and the multifunctionality of the platform, additionally the authors reported for the amperometric monitoring of intracellular redox activity in yeast (*Saccharomyces cerevisiae*), and detection of exocytotically released dopamine from rat pheochromocytoma cells. As mentioned previously, the electrical sensors seem to be more appropriate for easy integration on μTAS development. We shall consider in the following sections the most widely used techniques such as potentiometry, amperometry or voltammetry, and impedance spectroscopy. Concerning the latter, the advantages of contactless microelectrodes integration on-a-chip for impedance measurement and recent applications are discussed.

3.3.3. Potentiometry

We only discuss some potentiometric microsystems, i.e., the systems that have been manufactured at least partly using photolithography or other micromachining techniques and incorporate electrical or electrochemical measurement. This definition excludes a large group of potentiometric electrochemical sensors using microelectrodes. The reason for this exclusion is that the microelectrodes are a smaller version of their macroscopic analogue and their function is similar to larger electrode [101]. From the practical point of view, a potentiometric transducer within microsystem should include a conductive contact, a reference electrode and a microchannel for the fluid flow over the sensing surfaces [102].

Microfabrication of potentiometric sensors has several advantages over conventional electrodes, in particular by the dimensions of the measuring system, which is less expensive [103]. Indeed, emergence of lab-on-a-chip applications have benefited from the development of potentiometric sensors on small surfaces in contact with fluidic. Microfluidic systems with potentiometric detection have been developed and characterized. Among them, it can be mentioned the microanalyzer prototypes based on potentiometric measurements for various applications in analytical chemistry and biochemistry, such as ions detection [104], proteins [105], and Ph [106, 107]. The achievement of receptors based on low temperature co-fired ceramic or LTCC for potentiometric microsystems (called μPOT) offers good electrical and mechanical properties, as well as reliability and stability measures. Schöning et al. [108] developed potentiometric microsensor porous silicon, where microporous layer is formed by electrochemical etching. Thus, the microstructured surface allows the enlargement of the active area of the microsensor, which increases the measured capacitance. For instance Lakard et al. [107] developed potentiometric pH microsensors based on films of electrosynthesized polypyrrole, whose electrodes are fabricated by photolithography. The study showed that thin polypyrrole films present the best potentiometric linear responses in pH in the range of 2–11.

3.3.4. Amperometry and voltammetry

Amperometry and voltammetry techniques use the measurement of the electric current response of a working electrode against the applied potential in the electrochemical cell. The amperometric transductions within microdevices have wide applications in biosensing [109, 110]. Research in biosensors domain using amperometric sensors were initiated by Clark in 1956 by studying the oxygen electrodes [111]. In amperometric microsystems, the current measured with high sensitivity is linearly dependent on the concentration to be detected. This sensitivity is highlighted in the work of Pijanowska et al. [95] about the detection of glucose. These biosensors also have the advantage of being faster, cheaper, and more available than conductimetric and potentiometric biosensors [109]. Other studies have focused on the measurement of enzyme activity measured within miniaturized amperometric and voltammetric cells, using grafted proteins on the surface of the microelectrodes. These microdevices have the characteristic to give fast response [110]. The results showed a high linearity between the measured responses of the biosensor and the concentrations of the sample. Furthermore, microsystems in amperometric and voltammetric transduction have been successfully adapted

in capillary electrophoresis, conducted in a chip for toxicity detection of phenolic compounds [112] and synthetic food colorants [113].

The integration of a reference microelectrode in a microfluidic chip is often a hard step. Recently, Faure et al. [72] have proposed an alternative strategy requiring less microfabrication steps according to a configuration with two microelectrodes for electrochemical detection in glass/PDMS microfluidic chips. As displayed in Figure 10(b), it consists of using two micro-band electrodes of the same material with a surface ratio of 22 for the counter-electrode (S = 0.31 mm^2) with respect to the working microelectrode area (S = 0.014 mm^2). Therefore, the counter-electrode can be considered as a pseudo-reference since the current density flowing through it is much smaller than that flowing in the working electrode, thus, limiting possible variations on the rest of potentials. To this end, the redox couple $[Fe(III)(CN)6]^{3-}$/[Fe (II) $(CN)6]^{4-}$ is used to impose a 0 V as reference potential (see Figure 10). The chip performance using this geometry has been characterized using cyclic voltammetry according to the hydrodynamic conditions in chip, while differential pulse voltammetry (DPV) as it appears in Figure 10, with regard to its analytical performance was preferred for the LOD of transthyretin (TTR). The quantification of transthyretin peptide is a major interest for the diagnosis of familial amyloid polyneuropathy at transthyretin (ATTR) [114]. The obtained LOD for the TTR was determined at 25 nM, a value of 100-fold lower than that reported in conventional capillary electrophoresis coupled to the laser-induced fluorescence (LIF) under the same experimental conditions [115].

3.3.5. Electrical impedance spectroscopy

The electrochemical impedance spectroscopy is a well-established technique. Thus, the need to access to more sensitive and more precise measurements within microdevices opened novel strategies for sensor development that enable integration of electrical or electrochemical impedance spectroscopy. Among the areas where the impedance measurements are the most used, its noninvasive characteristic is crucial for many applications such as for counting, identification, and detection of particles or cells in biology and biochemistry [116]. In the last years, impedance measurements in microsystems have been mainly pursued to measure the electrical conductivity of liquid [117], the dielectric properties of the particles in suspension or in flow [116, 118], the properties of the cell membranes [119], the kinetics of enzymatic reactions [120], and the adsorption of red bloods on the sensor surfaces [121]. For instance, Park et al. [122] have improved a microfluidic device developed earlier by Ferrier et al. [123]. The microdevice was used for the detection of polystyrene microbeads and cancerous cells. In brief, the device comprised a microfluidic channel and two parallel planar electrodes for particles (microbeads and cells) actuation using dielectrophoresis (DEP), and a trap reservoir containing the electrodes for the impedance measurements. The study showed that measured impedance variations were in relation to the trapping and release of the microbeads and the cell in the reservoir. Ayliffe et al. [124] have also demonstrated the ability to detect the presence of a single particle using flow cytometry combined with the impedance measurement in a microfluidic device. The principle consists in measuring the electric impedance at the passage of a particle or a cell through a microchannel with electrodes disposed on its surface in order to detect each

http://dx.doi.org/10.5772/65772

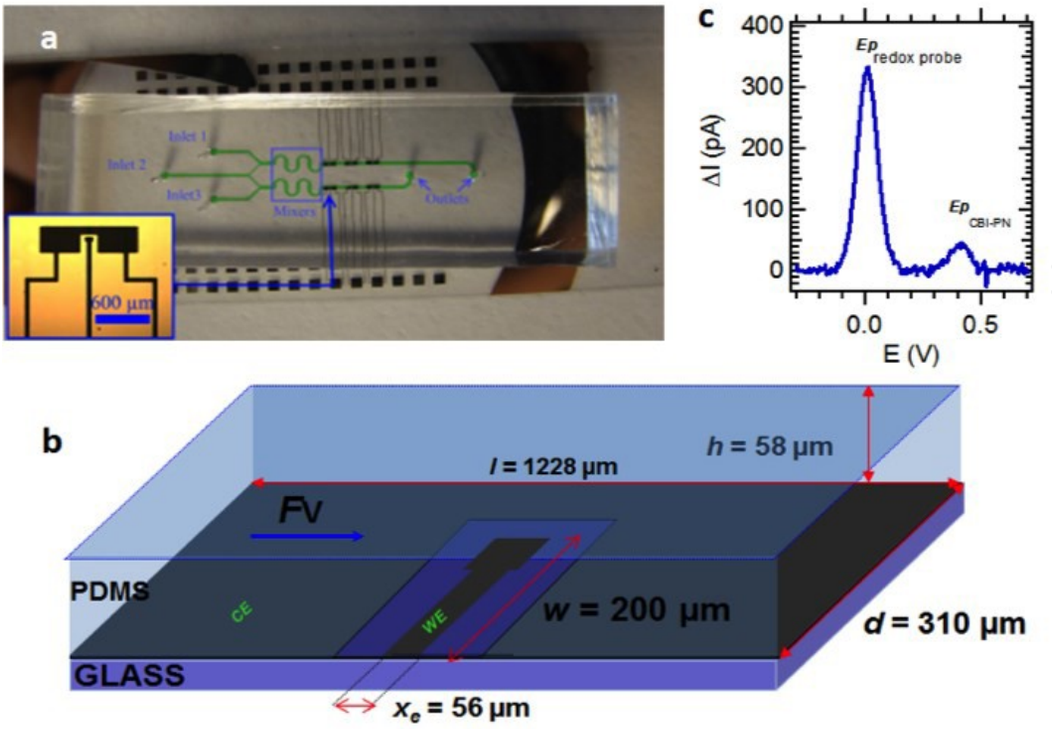

Figure 10. (a) Picture of several pairs of two microelectrodes networks located on the microchannel junction for multi-detection possibility. The fluidic microchannels allowing the sample injection with several configurations (inlet 1, 2, 3). (b) Schematic view of the detection area with a pair of microelectrodes (CE, counter electrode, WE, working electrode). The fluidic channel, WE, and CE microband electrodes characteristic dimensions: *h*, *d*, *w*, *x*e, and *l* are indicated and the B scheme is not to the scale. (c) Differential pulse voltammetry of 25 µm Transthyretin peptide (CBI-PN) in the presence of 1 mm $[Fe(III)(CN)6]^{3-}$/$Fe(II)(CN)6]^{4-}$ redox couple as potential reference in buffer 100 mm borate pH 9/MeOH (50/50, v/v). Scan rate 25 mV s^{-1} modulation time 100 ms modulation amplitude 7.5 mV under a flow rate of 0.05 µL s^{-1} from [72].

particle flowing [125]. Hediger et al. [126] have investigated on microfluidic devices for detection using impedance spectroscopy in the medical domain. The microdevice was achieved by plasma etching on a silicon substrate with platinum electrodes for detection. The preliminary test in case of device filled with sodium chloride at various concentrations underlined that the measured impedance module plateaus recorded between 10 kHz and 100 Hz decreased with an increase of NaCl concentration. As they expected, the resistance of the microchannel was found as being conversely proportional to solution conductivity.

In the last decades, other kinds of microdevices were developed with electrodes in contactless configuration with the electrolyte [128, 129]. The latter have emerged to overcome some limitations due to microelectrodes contamination, corrosion, or degradation [130]. In the next part, we focus on this original electrode configuration for which the start-of-art and the advantages are discussed for sensing and biosensing development.

Microfluidic chips with a detection module in noncontact mode have the particularity of having galvanically isolated microelectrodes embedded in a dielectric layer. The configuration in noncontact mode has several advantages in comparison with the traditional mode in contact. The encountered inconvenience for solution with microelectrode in contact is

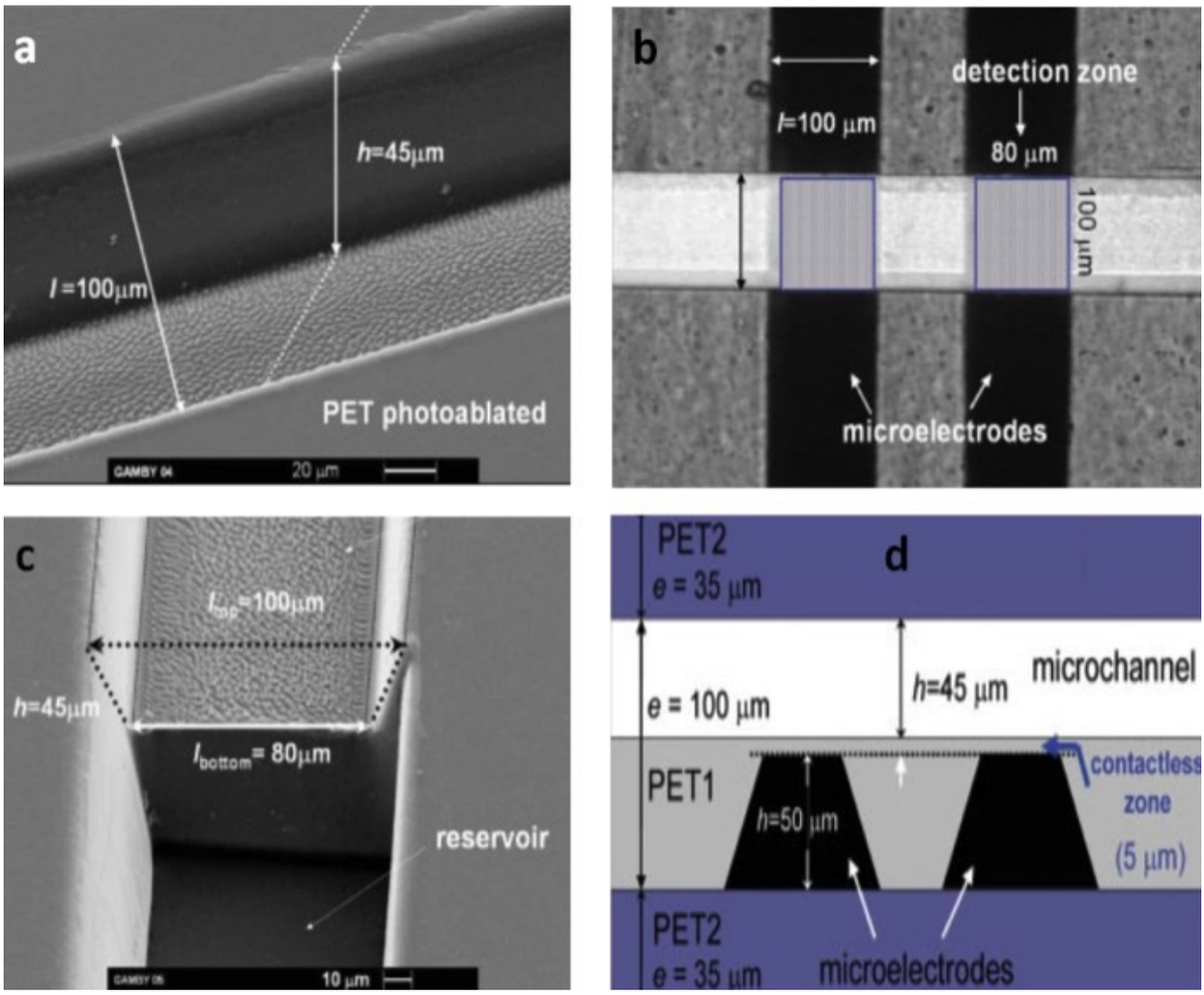

Figure 11. (a) Scanning electron microscopy (SEM) images of the PET photoablated microchannel with a cross- section of 45 × 100 μm and a length of 1.4 cm. (b) Optical image of the detection zone global view including the planar microelectrodes (inverted optical microscope), vertically, the two band electrodes beneath the horizontal flow channel. The detection zone represents the area where capacitive coupling takes place. (c) The SEM image of the trapezoidal section of the microchannel. (b) Side view of the contactless zone, which is about 5 μm and represents the thickness separation between the flow microchannel and the planar microelectrodes [127].

avoided, for instance, the microelectrode passivation or corrosion, the bubble generation due to uncontrolled faradic reactions on electrodes [132]. The first configuration of photoablated polyethylene terephthalate PET as flexible microchips with microelectrodes galvanically isolated into the PET was patented in 2004 [133], and then published by Gamby et al. [127]. Indeed, this system was called "SuperCapacitive Admittance Tomoscopy" (SCAT), based on the observation of a thin solvent layer on a dielectric thin film through two embedded microband electrodes (Figure 12). Indeed, the PET dielectric layer coating the two parallel microelectrodes contains a microchannel with chemically modified surface for adsorption of biomolecules [134].

The study is carried out by applying an alternating voltage of 0.1–3 V in the high frequencies (1 kHz–10 MHz) between the two microelectrodes. Indeed, a capacitive coupling effect appears

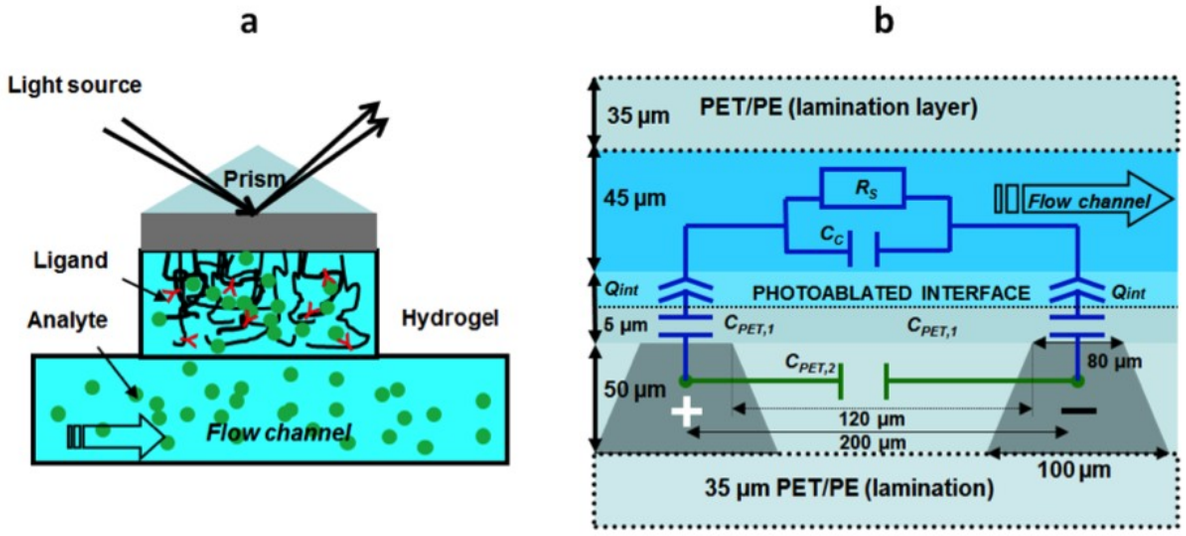

Figure 12. (a) Schematic representation of the BIACORE optical biosensor. The hydrogel is 100 nm high approximately. The ligand is immobilized in the hydrogel the analyte flows in the channel and diffuses in the gel where it binds to the ligand. (b) Cross-section of the dielectric interface microelectrode/ PET/ microchannel and the corresponding electrical equivalent circuit: $C_{PET,2}$ for the 120 µm-PET layer impedance (distance separation), $C_{PET,1}$ for the 5 µm-PET layer impedance (noncontact layer thickness), the element CPE, Qint, for the interfacial impedance (photoablated surface) [134].

through the dielectric layer, on the microelectrodes hand with electronic charges and on the other hand with microchannel filled with ionic charges. This enables the admittance measurement, which is itself related to the surface state of the PET chemically modified. The SCAT is suitable for the real-time study of electrostatic interactions analyte/substrate on any dielectric having a modified surface. Gamby et al. [127] have investigated the microchannel internal surface modification in the noncontact microdevice and they have showed that the surface charge can be turned and provides an opportunity to enhance the polymer-protein interactions. For instance, adsorption of β-Lactoglobulin in PET microchannel modified (poly(L-lysine) (PLL) adsorbed on gold nanoparticles bearing thiol-carboxylate functions) has been studied in the range of high-frequencies from 1 MHz to 1 kHz with an amplitude of 0.5 V, and finally, an LOD of 4.5×10^{-16} M was reported. The proof of concept of affinity biosensor development by using dielectric impedance detection on insulating PET was investigated and compared to an optical transduction such as surface plasmon resonance (SPR) illustrated on Figure 12 [131]. Proteins are not labeled, as in optical biosensor, even if they need to be attached to the polymer surface coupled with the microelectrodes when a biomolecular interaction occurs. As displayed in Figure 12, modeling the microchip interface using an appropriate equivalent circuit permits to extract the value of the interfacial capacitance for ultra-low protein concentration. The promising results obtained with this methodology make it a competing method in comparison with other transductions for bioanalytical developments. The equilibrium association constant was calculated for the affinity between the probe and the target and was estimated equal to 5×10^{7} M^{-1} in agreement with the one determined with SPR technique [78]. The promising results obtained with this strategy make it a competitive biosensor in comparison with SPR.

4. Conclusion

The development of a microfluidic system involves a myriad of issues and the proper selection of pertinent strategies regarding the overall feasibility, fabrication processes and targeted detection goals. At a starting point, due to its sensitivity and unfortunately, due to the fact that many materials platform and their related fabrication and conditioning means are yet be clearly identified and developed as a protocol, the coupled materials and fabrication relationship should be one of the top priorities. Undoubtedly, the most significant concern should be oriented toward the adaptation of the bioassay protocol in the specific microfluidic format, at this stage the robustness and the stability of the microfluidic operability should be taken into account in order to efficiently contribute to novel successful collaborations between different biologists, clinicians and the microfluidic communities.

Author details

Emmanuel Roy, Antoine Pallandre, Bacem Zribi, Marie-Charlotte Horny,
François-Damien Delapierre, Andrea Cattoni, Jean Gamby and Anne-Marie Haghiri-Gosnet*

*Address all correspondence to: anne-marie.haghiri-gosnet@lpn.cnrs.fr

Centre for Nanoscience and Nanotechnology, CNRS, University Paris Sud, University Paris Saclay, Marcoussis, France

References

[1] A. Arora, G. Simone, G. B. Salieb-Beugelaar, J. Tae Kim and A. Manz, Latest developments in micro total analysis systems, *Anal. Chem.*, 82, 4830–47, 2010.

[2] L. Gervais, N. de Rooij and E. Delamarche, Microfluidic chips for point-of-care immunodiagnostics, *Adv. Mater.*, 23, H151–76, 2011.

[3] N. T. Tran, I. Ayed, A. Pallandre and M. Taverna, Recent innovations in protein separation by electrophoretic methods: An update, *Electrophoresis*, 31, 147–73, 2010.

[4] M. Goto and M. N. Al-Hasan, Overall burden of bloodstream infection and nosocomial bloodstream infection in North America and Europe, *Clin. Microbiol. Infect.*, 19(6), 501–9, 2013.

[5] A. Kumar, D. Roberts, K. E. Wood, B. Light, J. E. Parrillo and S. S. Sharma, Duration of hypotension before initiation of effective antimicrobial therapy is the critical determinant of survival in human septic shock, *Crit. Care Med.*, 34(6), 1589–96, 2006.

[6] R. P. Dellinger, M. N. Levy, A. Rhodes, D. Annane, H. Gerlach and S. M. Opal, Surviving sepsis campaign: International guidelines for management of severe sepsis and septic shock, *Intensive Care Med*., 39(2), 165–228, 2013.

[7] M. E. de Kraker, V. Jarlier, J. C. Monen, O. E. Heuer, N. van de Sande and H. Grundmann, The changing epidemiology of bacteraemias in Europe: trends from the European Antimicrobial Resistance Surveillance System, *Clin. Microbiol. Infect*., 19(9), 860–8, 2013.

[8] E. J. Baron, M. P. Weinstein, W. M. Dunne, P. Yagupsky, D. F. Welch, D. M. Wilson and C. Cumitech, *Blood Cultures IV*. ASM Press, 2005, Washington, DC. 3.

[9] C. Pautas, E. Sbidian, Y. Hicheri, S. Bastuji-Garin, S. Bretagne and C. Corbel, A new workflow for the microbiological diagnosis of febrile neutropenia in patients with a central venous catheter, *J. Antimicrob. Chemother*., 68(4), 943–6, 2012.

[10] C. Brun-Buisson, P. Meshaka, P. Pinton, B. Vallet, EPISEPSIS: A reappraisal of the epidemiology and outcome of severe sepsis in French intensive care units, *Intensive Care Med*., 30(4), 580–8, 2004.

[11] K. Reinhart, M. Bauer, N. C. Riedemann and C. S. Hartog, New approaches to sepsis: molecular diagnostics and biomarkers, *Clin. Microbiol. Rev*., 25(4), 609–34, 2012.

[12] R. Yang, J. V. Pagaduan, M. Yu and A. T. Woolley, On chip preconcentration and fluorescence labeling of model proteins by use of monolith columns: Device fabrication, optimization and automation, *Anal. Bioanal. Chem*., 407, 737–747, 2015.

[13] J. A. Lounsbury, A. Karlsson, D. C. Miranian, S. M. Cronk, D. A. Nelson, J. Li, D. M. Haverstick, P. Kinnon, D. J. Saul and J. P. Landers, From sample to PCR product in under 45 minutes: A polymeric integrated microdevice for clinical and forensic DNA analysis, *Lab Chip*, 13, 1384–93, 2013.

[14] R. Zhong, D. Liu, L. Yu, N. Ye, Z. Dai, J. Qin and B. Lin, Fabrication of two-weir structure-based packed columns for on-chip solid-phase extraction of DNA, *Electrophoresis*, 28(16), 2920–26, 2007.

[15] J. West, M. Boerlin, A. D. Jadhav and E. Clancy, Silicon microstructure arrays for DNA extraction by solid phase sample contacting at high flow rates, *Sens. Actuators B*, 126, 664–71, 2007.

[16] M. B. Dainiak, I. Y. Galaev, A. Kumar, F. M. Plieva and B. Mattiasson, Chromatography of living cells using supermacroporous cryogels, *Adv. Biochem. Eng. Biotechnol*., 106, 101–27, 2007.

[17] H. Chen, Q. Fang, X. F. Yin and Z. L. Fang, Microfluidic chip-based liquid-liquid extraction and preconcentration using a subnanoliter-droplet trapping technique, *Lab Chip*, 5(7), 719–25, 2005.

[18] A. Aota, M. Nonaka, A. Hibara and T. Kitamori, Countercurrent laminar microflow for highly efficient solvent extraction, *Angew. Chem. Int. Ed*., 46, 878–80, 2007.

[19] T. Minagawa, M. Tokeshi and T. Kitamori, Integration of a wet analysis system on a glass chip: Determination of Co(II) as 2-nitroso-1-naphthol chelates by solvent extraction and thermal lens microscopy, *Lab Chip*, 1, 72–5, 2001.

[20] H. Miyaguchi, M. Tokeshi, Y. Kikutani, A. Hibara, H. Inoue and T. Kitamori, Microchip-based liquid-liquid extraction for gas-chromatography analysis of amphetamine-type stimulants in urine, *J. Chromatogr. A*, 1129, 105–10, 2006.

[21] A. Smirnova, K. Shimura, A. Hibara, M. A. Proskurnin and T. Kitamori, Pesticide analysis by MEKC on a microchip with hydrodynamic injection from organic extract, *J. Sep. Sci*., 31, 904–8, 2008 (Special Issue: *Micellar Electrokinetic Chromatography*).

[22] V. Reddy and J. D. Zahn, Interfacial stabilization of organic-aqueous two-phase microflows for a miniaturized DNA extraction module, *J. Colloid Interface Sci.*, 286, 158–65, 2005.

[23] N. Assmann, A. Ladosz and P. R. von Rohr, Continous micro liquid-liquid extraction (Review), *Chem. Eng. Technol.*, 36(6), 921–36, 2013.

[24] S. G. Redkar and R. H. Davis, Cross-flow microfiltration *with* high-frequency reverse filtration, *AlChE J*., 41, 501–8, 1995.

[25] M.-C. Lo and J. D. Zahn, Development of a multi-compartment microfiltration device for particle fractionation, 16th international conference on miniaturized systems for chemistry and life sciences, Okinawa, Japan, 2012.

[26] K. Aran, A. Fok, L. A. Sasso, N. Kamdar, Y. Guan, Q. Sun, A. Ündar and J. D. Zahn, Microfiltration platform for continuous blood plasma protein extraction from whole blood during cardiac surgery, *Lab Chip*, 11, 2858–68, 2011.

[27] K. Aran, M. Morales, L. A. Sasso, J. Lo, J. Zheng, I. Johnson and J. D. Zahn, Microflitration device for continuous label-free bacteria separation from whole blood for sepsis, the 15th international conference on miniaturized systems for chemistry and life sciences, MicroTAS, 2011.

[28] J. Chung, H. Shao, T. Reiner, D. Issadore, R. Weissleder and H. Lee, Microfluidic cell sorter (μFCS) for on-chip capture and analysis of single cells, *Adv. Healthc. Mater*., 1(4), 432–6, 2012.

[29] H. Mohamed, M. Murray, J. N. Turner and M. Caggana, Isolation of tumor cells using size and deformation, *J. Chromatogr. A,* 1216, 8289–95, 2009.

[30] D. Lee, P. Sukuma, A. Mahyuddin, M. Choolani and G. Xu, Separation of model mixtures of ε-globin positive fetal nucleated red blood cells and a nucleate erythrocytes using a microfluidic device, *J. Chromatogr. A*, 1217(11), 1862– 66, 2010.

[31] S. K. Murthy, P. Sethu, G. Vunjak-Novakovic, M. Toner and M. Radisic, Size-based microfluidic enrichment of neonatal rat cardiac cell populations, *Biomed. Microdevices.*, 8(3), 231–37, 2006.

[32] S. Tripathi, Y. V. Bala Varun Kumar, A. Prabhakar, S. S. Joshi and A. Agrawal, Passive blood plasma separation at the microscale: A review of design principles and microdevices, *J. Micromech. MicroEng.*, 25, 083001, 2015.

[33] P. Sajeesh and A. Kumar Sen, Particle separation and sorting in microfluidic devices: A review, *Microfluid. Nanofluid.*, 17, 1–52, 2014.

[34] L. R. Huang, E. C. Cox, R. H. Austin and J. C. Sturm, Continuous particle separation through deterministic lateral displacement, *Science*, 304, 987–90, 2004.

[35] J. Zhou and I. Papautsky, Fundamentals of inertial focusing in microchannels, *Lab Chip*, 13(6), 1121–32, 2013.

[36] D. Di Carlo, Inertial microfluidics, *Lab Chip*, 9, 3038–46, 2009.

[37] D. Di Carlo, D. Irimia, R. G. Tompkins and M. Toner, Continuous inertial focusing, ordering, and separation of particles in microchannels. *PNAS,* 104(48), 18892–97, 2007.

[38] J. McGrath, M. Jimenez and H. Bridle, Deterministic lateral displacement for particle separation: A review, *Lab Chip*, 14, 4139–58, 2014.

[39] D. W. Inglis, Efficient microfluidic particle separation arrays, *Appl. Phys. Lett.*, 94(1), 013510, 2009.

[40] K. Loutherback, K. S. Chou, J. Newman, J. Puchalla and R. H. Austin, Improved performance of deterministic lateral displacement arrays with triangular posts, *Microfluid. Nanofluid.*, 9(6), 1143–49, 2010.

[41] K. Loutherback, J. D'Silva, L. Liu, A. Wu, R. H. Austin and J. C. Sturm, Deterministic separation of cancer cells from blood at 10 mL/min, *AIP Adv.*, 2(4), 042107, 2012.

[42] K. K. Zeming, S. Ranjan and Y. Zhang, Rotational separation of non-spherical bioparticles using I-shaped pillar arrays in a microfluidic device, *Nat. Commun.*, 4, 1625, 2013.

[43] M. Al-Fandi, M. Al-Rousan, M. A. Jaradat and L. Al-Ebbini, New design for the separation of microorganisms using microfluidic deterministic lateral displacement, *Robot. Comput. Integr. Manuf.*, 27, 237–44, 2011.

[44] R. Fan, O. Vermesh, A. Srivastava, B. K. H. Yen and L. Qin L, Integrated barcode chips for rapid, multiplexed analysis of proteins in microliter quantities of blood, *Nat. Biotechnol.*, 26(12), 1373–78, 2008.

[45] J. M. Martel and M. Toner, Inertial focusing in microfluidics, *Annu. Rev. Biomed. Eng.*, 16(1), 371–96, 2014.

[46] M. E. Warkiani, G. Guan, K. B. Luan and A. A. S. Bhagat, Slanted spiral microfluidics for the ultra-fast, label-free isolation of circulating tumor cells, *Lab Chip*, 14, 128–37, 2014.

[47] L. Clime, X. D. Hoa, N. Corneau, K. J. Morton, C. Luebbert, M. Mounier, D. Brassard, M. Geissler, S. Bidawid, Jeff Farber and T. Veres, Microfluidic filtration and extraction of pathogens from food samples by hydrodynamic focusing and inertial lateral migration, *Biomed. Microdevices*, 17, 17, 2015.

[48] J. H Kang, M. Super, C. Wing Yung, R. M. Cooper, K. Domansky, A. R. Graveline, T. Mammoto, J. B. Berthet, H. Tobin, M. J. Cartwright, A. L. Watters, M. Rottman, A. Waterhouse, A. Mammoto, N. Gamini, M. J. Rodas, A. Kole, A. Jiang, T. M. Valentin, A. Diaz, K. Takahashi and Donald E Ingber, An extracorporeal blood-cleansing device for sepsis therapy, *Nat. Med.*, 20(10), 1211–21, 2014.

[49] H. J. Hjertén, Free zone electrophoresis, *Chromatogr. Rev.*, 9, 122–219, 1967.

[50] "Capillary Electrophoresis Methods and Protocols" Editors: Schmitt-Kopplin, Philippe (Ed.) 2008 Springer ISBN 978-1-59745-376-9, Humana Press Inc, Totowa, NJ.

[51] "Capillary Electrophoresis and Microchip Capillary Electrophoresis: Principles, Applications, and Limitations", Carlos D. Garcia, Karin Y. Chumbimuni-Torres, Emanuel Carrilho 2013 Wiley, San Antonio, TX, USA, ISBN: 978-0-470-57217-7

[52] A. Manz, N. Graber and H. M. Widmer, Miniaturized total chemical analysis systems: A novel concept for chemical sensing, *Sens. Actuators B Chem.*, 1(1), 244–48, 1990.

[53] J. W. Jorgenson and K. D. Lukacs, Capillary zone electrophoresis, *Science*, 222, 266–72, 1983.

[54] A. Pallandre, B. de Lambert, R. Attia, A. M. Jonas, J.-L. Viovy, Surface treatment and characterization: Perspectives to electrophoresis and Lab-on-Chips, *Electrophoresis*, 27, 584–610, 2006.

[55] R. B. M. Schasfoort, S. Schlautmann, L. Hendrikse and A. van den Berg, Field-effect flow control for microfabricated fluidic networks, *Science*, 286, 942–45, 1999.

[56] A. Plecis, J. Tazid, A. Pallandre, P. Martinhon, C. Deslouis, Y. Chen and A. M. Haghiri-Gosnet, Flow field effect transistors with polarisable interface for EOF tunable microfluidic separation devices, *Lab Chip*, 10, 1245–53, 2010.

[57] R. Liedert, L. K. Amundsen, A. Hokkanen, M. Mäki, A. Aittakorpi, M. Pakanen, J. R. Scherer, R. A. Mathies, M. Kurkinen, S. Uusitalo, L. Hakalahti, T. K. Nevanen, H. Siitari and H. Söderlund, Disposable roll-to-roll hot embossed electrophoresis chip for detection of antibiotic resistance gene *mecA* in bacteria, *Lab Chip*, 12, 333–39, 2012.

[58] Q. Pu, J. Yun, H. Temkin and S. Liu, Ion-enrichment and ion-depletion effect of nanochannel structures, *Nano Lett.*, 4, 1099–1103, 2004.

[59] T. A. Zangle, A. Mani and J. G. Santiago, Theory and experiments of concentration polarization and ion focusing at microchannel and nanochannel interfaces, *Chem. Soc. Rev.*, 39, 1014–35, 2010.

[60] A. C. Louer, A. Plecis, A. Pallandre, J. C. Galas, A. Estevez-Torres and A. M. Haghiri-Gosnet, Pressure-assisted selective preconcentration in a straight nanochannel, *Anal. Chem.*, 85, 7948, 2013.

[61] S. Mehrabani, A. J. Maker and A. M. Armani, Hybrid integrated label-free chemical and biological sensor, *Sensors*, 14, 5890–928, 2014.

[62] K. V. Gobi, H. Iwasaka and N. Miura, Self-assembled PEG monolayer based SPR immunosensor for label-free detection of insulin, *Biosens. Bioelectron*., 22, 1382–89, 2007.

[63] K. V. Gobi, S. J. Kim, H. Tanaka, Y. Shoyama and N. Miura, Novel surface plasmon resonance (SPR) immunosensor based on monomolecular layer of physically-adsorbed ovalbumin conjugate for detection of 2,4-dichlorophenoxyacetic acid and atomic force microscopy study, *Sens. Actuators* B, 123, 583–93, 2007.

[64] K. S. Kim, H.-S. Lee, J.-A. Yang, M.-H. Jo and S. K. Hahn, The fabrication, characterization and application of aptamer-functionalized Si-nanowire FET biosensors, *Nanotechnology*, 20, 235501, 2009.

[65] T. P. Burg, M. Godin, S. M. Knudsen, W. Shen, G. Carlson, J. S. Foster, K. Babcock and S. R. Manalis, Weighing of biomolecules, single cells and single nanoparticles in fluid, *Nature*, 446, 1066–69, 2007.

[66] S. B. Patil, M. Vögtli, B. Webb, G. Mazza, M. Pinzani, Y-A. Soh, R. A. McKendry and J. W. Ndieyira, Decoupling competing surface binding kinetics and reconfiguration of receptor footprint for ultrasensitive stress assays, *Nat. Nanotechnol.*, 10, 899–907, 2015.

[67] H. C. Tekin and M. A. M. Gijs, Ultrasensitive protein detection: A case for microfluidic magnetic bead-based assays, *Lab Chip*, 13, 4711–39, 2013.

[68] R. S. Gaster, D. A. Hall, C. H. Nielsen, S. J. Osterfeld, H. Yu, K. E. Mach, R. J. Wilson, B. Murmann, J. C. Liao, S. S. Gambhir and S. X. Wang, Matrix-insensitive protein assays push the limits of biosensors in medicine, *Nat. Med.*, 15, 1327–32, 2009.

[69] I. Lignos, S. Stavrakis, A. Kilaj and A. J. deMello, Millisecond-timescale monitoring of PbS nanoparticle nucleation and growth using droplet-based microfluidics, *Small*, 11(32), 4009–17, 2015.

[70] S. Mandal, J. M. Goddard and D. Erickson, A multiplexed optofluidic biomolecular sensor for low mass detection, *Lab Chip*, 9, 2924–32, 2009.

[71] T. L. Edwards, J. C. Harper, R. Polsky, D. M. Lopez, D. R. Wheeler, A. C. Allen and S. M. Brozik, A parallel microfluidic channel fixture fabricated using laser ablated plas-

tic laminates for electrochemical and chemiluminescent biodetection of DNA, *Biomicrofluidics*, 5,044115,2011.

[72] M. Faure, A. Pallandre, S. Chebil, I. Le Potier, M. Taverna, B. Tribollet, C. Deslouis, A.-M. Haghiri-Gosnet and J. Gamby, Improved electrochemical detection of a transthyretin synthetic peptide in the nanomolar range with a two-electrode system integrated in a glass/PDMS microchip, *Lab Chip*, 14, 2800–05, 2014.

[73] J. L. Arlett, E. B. Myers and M. L. Roukes, Comparative advantages of mechanical biosensors, *Nat. Nanotechnol*. 6, 203–15, 2011.

[74] N. Pamme, Magnetism and microfluidics, *Lab Chip*, 6, 24–38, 2006.

[75] C. Monat, P. Domachuk and B. J. Eggleton, Integrated optofluidics: A new river of light, *Nat. Photon.*, 1, 106– 114, 2007.

[76] D. Psaltis, S. R. Quake and C. Yang, Developing optofluidic technology through the fusion of microfluidics and optics, *Nature*, 442, 381–86, 2006.

[77] A. G. Brolo, Plasmonics for future biosensors, *Nat. Photon.*, 6, 709–13, 2012.

[78] A. Kausaite, M. van Dijk, J. Castrop, A. Ramanaviciene, J. P. Baltrus, J. Acaite and A. Ramanavicius, Surface plasmon resonance label-free monitoring of antibody antigen interactions in real time, Biochem. Mol. Boil. Educ., 35, 57–63, 2007.

[79] C. Y. Chao, L. J. Guo, Biochemical sensors based on polymer microrings with sharp asymmetrical resonance, *Appl. Phys. Lett*., 83, 1527–29, 2003.

[80] D. K. Armani, T. J. Kippenberg, S. M. Spillane and K. J. Vahala, Ultra-high-Q toroid microcavity on a chip, *Nature*, 421, 925–28, 2003.

[81] T. J. Kippenberg, S. M. Spillane, D. K. Armani and K. J. Vahala, Fabrication and coupling to planar high-Q silica disk microcavities, *Appl*. *Phys*. *Lett*., 83, 797–99, 2003.

[82] J. Niehusmann, A. Vörckel, P. H. Bolivar, T. Wahlbrink, W. Henschel and H. Kurz, Ultrahigh-quality-factor silicon-on-insulator microring resonator, *Opt. Lett.*, 29, 2861–63, 2004.

[83] M. Loncar, A. Scherer and Y. Qiu, Photonic crystal laser sources for chemical detection, *Appl*. *Phys*. *Lett*., 82, 4648–4650, 2003.

[84] X. Fan, I. M. White, S. I. Shopova, H. Zhu, J. D. Suter and Y. Sun, Sensitive optical biosensors for unlabeled targets: A review, *Anal. Chim. Acta*, 620, 8–26, 2008.

[85] S. M. Borisov and O. S. Wolfbeis, Optical Biosensors, *Chem*. *Rev*., 108, 423−61, 2008.

[86] J. D. Joannopoulos and S. G. Johnson, Photonic crystals: Molding the flow of light, Princeton University Press, 2008, Princeton, New Jersey.

[87] C. Fenzl, T. Hirsch and O. S. Wolfbeis, Photonic crystals for chemical sensing and biosensing, *Angew*. *Chem*. *Int*. *Ed*., 53, 3318–35, 2014.

[88] D. Stuart, A. Haes, C. Yonzon, E. Hicks and R. P. Van Duyne, Biological applications of localised surface plasmonic phenomenae, *IEEE Proc. Nanobiotechnol*., 152, 13–32, 2005.

[89] M. Svedendahl, S. Chen, A. Dmitriev and M. Käll, Refractometric sensing using propagating versus localized surface plasmons: A direct comparison, *Nano Lett*., 9, 4428–33, 2009.

[90] A. Cattoni, P. Ghenuche, A.-M. Haghiri-Gosnet, D. Decanini, J. Chen, J.-L. Pelouard and S. Collin, $\lambda^3/1000$ plasmonic nanocavities for biosensing fabricated by soft UV nanoimprint Lithography, *Nano Lett.*, 11,3557 63, 2011.

[91] S. S. Acímovic, M. A. Ortega, V. Sanz, J. Berthelot, J. L. Garcia-Cordero, J. Renger, S. J. Maerkl, M. P. Kreuzer and R. Quidant, LSPR chip for parallel, rapid, and sensitive detection of cancer markers in serum, *Nano Lett*., 14, 2636−41, 2014.

[92] T. M Squires, R. J Messinger and S. R. Manalis, Making it stick: Convection, reaction and diffusion in surface-based biosensors, *Nat. Biotechnol*., 26, 417–26, 2008.

[93] J. S. Rossier, M. A. Roberts, R. Ferrigno and H. H. Girault, Electrochemical detection in polymer microchannels, *Anal. Chem*., 71, 4294–99, 1999.

[94] V. Tsouti, C. Boutopoulos, I. Zergioti and S. Chatzandroulis, Capacitive microsystems for biological sensing, *Biosens. Bioelectron*., 27, 1–11, 2011.

[95] D. G. Pijanowska, A. J. Sprenkels, W. Olthuis and P. Bergveld, A flow-through amperometric sensor for micro-analytical systems, *Sen. Actuators B: Chem*., 91, 98–102, 2003.

[96] S. E. Rosenwald, N. Dontha and W. G. Kuhr, A laser ablation method for the spatial segregation of enzyme and redox sites on carbon fiber microelectrodes, *Anal. Chem*., 70, 1133–40, 1998.

[97] J. S. Daniels and N. Pourmand, Label-free impedance biosensors: Opportunities and challenges, *Electroanalysis*, 19, 1239–57, 2007.

[98] B. S. Ferguson, S. F. Buchsbaum, J. S. Swensen, K. Hsieh, X. Lou and H. T. Soh, Integrated microfluidic electrochemical DNA sensor, *Anal. Chem*., 81, 6503−08, 2009.

[99] A. Bhimji, A. A. Zaragoza, L. S. Live and S. O. Kelley, Electrochemical enzyme-linked immunosorbent assay featuring proximal reagent generation: Detection of human immunodeficiency virus antibodies in clinical samples, *Anal. Chem*., 85(14), 6813–19, 2013.

[100] K. Zór, A. Heiskanen, C. Caviglia, M. Vergani, E. Landini, F. Shah, M. Carminati, A. Martínez-Serrano, T. Ramos Moreno, M. Kokaia, D. Benayahu, Z. Keresztes, D. Papkovsky, U. Wollenberger, W. E. Svendsen, M. Dimaki, G. Ferrari, R. Raiteri, M. Sampietro, M. Dufva and J. Emnéus, A compact multifunctional microfluidic platform for

exploring cellular dynamics in real-time using electrochemical detection, *RSC Adv.*, 4, 63761–71, 2014.

[101] J. Janata, Potentiometric microsensors, *Chem. Rev.*, 90, 691–3, 1990.

[102] S. A. Almeida, E. Arasa, M. Puyol, C. S. Martinez-Cisneros, J. Alonso-Chamarro, M. C. Montenegro and M. G. Sales, Novel LTCC-potentiometric microfluidic device for biparametric analysis of organic compounds carrying plastic antibodies as ionophores: Application to sulfamethoxazole and trimethoprim, *Biosens. Bioelectron.*, 30, 197–203, 2011.

[103] S. S. Hassan, H. E. Sayour and S. S. Al-Mehrezi, A novel planar miniaturized potentiometric sensor for flow injection analysis of nitrates in wastewaters, fertilizers and pharmaceuticals, *Anal. Chim. Acta*, 581, 13–18, 2007.

[104] N. Ibáñez-García, M. Baeza, M. Puyol, R. Gómez, M. Batlle and J. Alonso-Chamarro, Biparametric potentiometric analytical microsystem based on the green tape technology, *Electroanalysis*, 22, 2376–82, 2010.

[105] T. Ahuja, I. A. Mir and D. Kumar, Potentiometric urea biosensor based on BSA embedded surface modified polypyrrole film, *Sens. Actuators B: Chem.*, 134, 140–45, 2008.

[106] M. J. Natan, D. Belanger, M. K. Carpenter and M. S. Wrighton, pH-sensitive nickel(II) hydroxide-based microelectrochemical transistors, *J. Phys. Chem.*, 91, 1834–42, 1987.

[107] B. Lakard, O. Segut, S. Lakard, G. Herljem and T. Gharbi, Potentiometric miniaturized pH sensors based on polypyrrole films, *Sens. Actuators B: Chem.*, 122, 101–8, 2007

[108] M. J. Schöning, F. Ronkel, M. Crott, M. Thust, J. W. Schultze, P. Kordos and H. Lüth, Miniaturization of potentiometric sensors using porous silicon microtechnology, *Electrochim. Acta*, 42, 3185–93, 1997.

[109] S. V. Dzyadevych, V. N. Arkhypova, A. P. Soldatkin, A. V. El'skaya, C. Martelet and N. Jaffrezic-Renault, Amperometric enzyme biosensors: Past, present and future, *IRBM*, 29, 171–80, 2008.

[110] Y. Chao, H. Yue, B. L. Hassler, R. M. Worden and A. J. Mason, Amperometric electrochemical microsystem for a miniaturized protein biosensor array, biomedical circuits and systems, *IEEE Transactions on*, 3, 160–68, 2009.

[111] L. C. Clark, Monitor and control of blood and tissue oxygen tensions, *Trans. Am. Soc. Artif. Intern. Organs*, 2, 41, 1956.

[112] J. Wang, M. P. Chatrathi and B. Tian, Capillary electrophoresis microchips with thick-film amperometric detectors: separation and detection of phenolic compounds, *Anal. Chim. Acta*, 416, 9–14, 2000.

[113] N. Dossi, R. Toniolo, A. Pizzariello, S. Susmel, F. Perennes and G. Bontempelli, A capillary electrophoresis microsystem for the rapid in-channel amperometric detection of synthetic dyes in food, *J. Electroanal. Chem.*, 601, 1–7, 2007.

[114] M. Faure, S. Korchane, I. Le Potier, A. Pallandre, C. Deslouis, A.-M. Haghiri-Gosnet and J. Gamby, Investigating of labeling and detection of transthyretin synthetic peptide derivatized with naphthalene-2,3-dicarboxaldehyde, *Talanta*, 116, 8–13, 2013.

[115] S. Korchane, A. Pallandre, C. Przybylski, C. Poas, F. Gonnet, M. Taverna, R. Daniel and I. Le Potier, Derivatization strategies for CE-LIF analysis of biomarkers: toward a clinical diagnostic of familial transthyretin amyloidosis, *Electrophoresis*, 35, 1050–59, 2014.

[116] T. Sun and H. Morgan, Single-cell microfluidic impedance cytometry: a review, *Microfluid Nanofluid*, 8, 423–43, 2010.

[117] F. Opekar, P. Tůma and K. Štulík, Contactless impedance sensors and their application to flow measurements, *Sensors*, 13, 2786–01, 2013.

[118] G. M. Dittami, H. E. Ayliffe, C. S. King and R. D. Rabbitt, A multilayer MEMS platform for single-cell electric impedance spectroscopy and electrochemical analysis, microactuators, microsensors, and microsystems : a joint IEEE and ASME publication on microstructures, *J. microelectromech.*, 17, 850–62, 2008.

[119] J. L. Hong, K. C. Lan, L. S. Jang, Electrical characteristics analysis of various cancer cells using a microfluidic device based on single-cell impedance measurement, *Sens. Actuators B: Chem*., 173, 927–934, 2012.

[120] M. Faure, M. Kechadi, B. Sotta, J. Gamby and B. Tribollet, Contact free impedance methodology for investigating enzymatic reactions into dielectric polymer microchip, *Electroanalysis*, 25, 1151–58, 2013.

[121] T. Sun, E. J. Swindle, J. E. Collins, J. A. Holloway, D. E. Davies and H. Morgan, On-chip epithelial barrier function assays using electrical impedance spectroscopy, *Lab Chip*, 10, 1611–17, 2010.

[122] H. Park, D. Kim and K. S. Yun, Single-cell manipulation on microfluidic chip by dielectrophoretic actuation and impedance detection, *Sens. Actuators B: Chem.*, 150, 167–73, 2010.

[123] G. A. Ferrier, A. N. Hladio, D. J. Thomson, G. E. Bridges, M. Hedayatipoor, S. Olson and M. R. Freeman, Microfluidic electromanipulation with capacitive detection for the mechanical analysis of cells, *Biomicrofluidics*, 2, 044102–13, 2008.

[124] H. E. Ayliffe, A. Bruno Frazier and R. D. Rabbitt, Electric impedance spectroscopy using microchannels with integrated metal electrodes, *J. Microelectromech. Syst*., 8, 50–57, 1999.

[125] M. Evander, A. J. Ricco, J. Morser, G. T. Kovacs, L. L. Leung and L. Giovangrandi, Microfluidic impedance cytometer for platelet analysis, *Lab Chip*, 13, 722–729, 2013.

[126] S. Hediger, A. Sayah and M. A. Gijs, Fabrication of a novel microsystem for the electrical characterisation of cell arrays, *Sens. Actuators B: Chem.*, 56, 175–80, 1999.

[127] J. Gamby, J. P. Abid, B. Tribollet and H. H. Girault, Nanomosaic network for the detection of proteins without direct electrical contact, *Small*, 4, 802–9, 2008.

[128] A. J. Zemann, E. Schnell, D. Volgger and G. K. Bonn, Contactless conductivity detection for capillary electrophoresis, *Anal. Chem.*, 70, 563–67, 1998.

[129] M. Pumera, Contactless conductivity detection for microfluidics: Designs and applications, *Talanta*, 74, 358–64, 2007.

[130] B. Gaš, M. Demjaněnko and J. Vacík, High-frequency contactless conductivity detection in isotachophoresis, *J. Chromatogr. A*, 192, 253–57, 1980.

[131] J. Gamby, J.-P. Abid and H. H. Girault, Supercapacitive admittance tomoscopy, *J. Am. Chem. Soc.*, 127, 13300–04, 2005.

[132] J. Gamby, J. P. Abid, M. Abid, J. P. Ansermet and H. H. Girault, Nanowires network for biomolecular detection using contactless impedance tomoscopy technique, *Anal. Chem*., 78, 5289–95, 2006.

[133] J.-P. Abid, J. O. Gamby and H. H. Girault, Adsorption monitoring device for contactless testing of sensors using capacitive admittance, *in, Ecole Polytechnique Federale de Lausanne, Switzerland* , p. 33, 2006.

[134] M. Kechadi, B. Sotta, L. Chaal, B. Tribollet and J. Gamby, A real time affinity biosensor on an insulated polymer using electric impedance spectroscopy in dielectric microchips, *Analyst*, 139, 3115–21, 2014.